Nucleic Acids Research, 2025, **53**, gkaf127
https://doi.org/10.1093/nar/gkaf127
Gene regulation, Chromatin and Epigenetics

Argonaute CSR-1A promotes H3K9me3 maintenance to protect somatic development in offspring

Di Rao[1,2,3,4], Dengfeng Li[2,3,4], Lili Li[2,3,4], Junchao Xue[2,3,4], Shikui Tu[5], En-Zhi Shen[2,3,4,*]

[1]Fudan University, Shanghai, China
[2]Key Laboratory of Growth Regulation and Transformation Research of Zhejiang Province, School of Life Sciences, Westlake University, Hangzhou, Zhejiang, China
[3]Westlake Laboratory of Life Sciences and Biomedicine, Hangzhou, Zhejiang, China
[4]Institute of Biology, Westlake Institute for Advanced Study, Hangzhou, Zhejiang, China
[5]Department of Computer Science and Engineering, Center for Cognitive Machines and Computational Health (CMaCH), Shanghai Jiao Tong University, Shanghai, China

[*]To whom correspondence should be addressed. Email: shenenzhi@westlake.edu.cn

Abstract

Parental stress can be encoded into altered epigenetic information to influence their offspring. Concurrently, it is vital for the preservation of a parent's epigenetic information, despite environmental challenges, to ensure accurate inheritance by the next generation. Nevertheless, the complexities of this process and the specific molecular mechanisms involved are not yet fully understood. Here we report that Argonaute CSR-1A potentiates the recovery of histone H3 lysine 9 trimethylation (H3K9me3) in spermatocyte to secure the developmental competence of male offspring. CSR-1A employs its repetitive RG motif to engage with putative histone 3 lysine 9 (H3K9) methyltransferases SET-25 and -32, and helps to restore repressive H3K9me3 chromatin marks following heat-stress, protecting the late development of somatic cells in the progeny. Finally, among the genes regulated by CSR-1A, we identified *dim-1*, at which decreased H3K9me3 persists in the progeny, and RNAi of *dim-1* mitigates the somatic defects associated with *csr-1a* loss under stress. Thus, CSR-1A coordinates a paternal epigenetic program that shields development from the influences of the paternal environment. We speculate that, driven by both natural environmental stressors and the unique characteristics of spermatogenic chromatin, the emergence of multiple RG motif-featured and spermatogenesis-specific CSR-1A and small RNA serves as a protective strategy to safeguard against variability in the orchestration of inherited developmental programs from the paternal lineage.

Graphical abstract

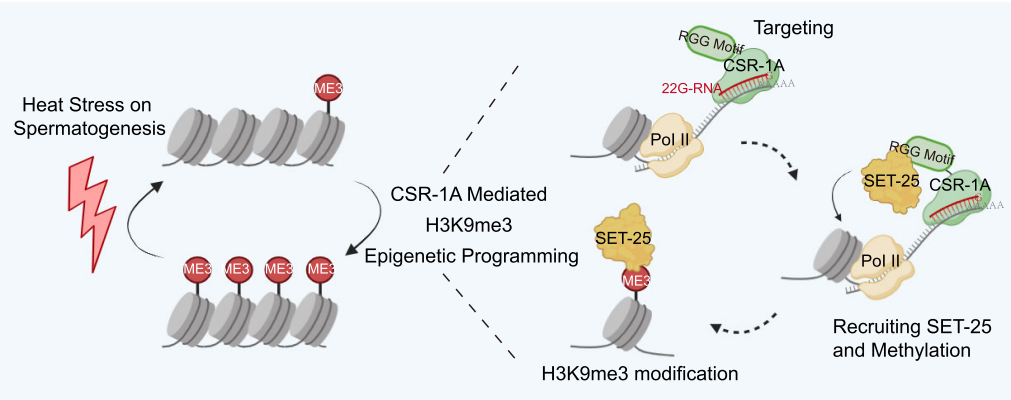

Introduction

The development and health of many organisms are greatly influenced by the environment [1–3]. Adaptation of parental exposure to environmental stressors ensures proper cellular responses and survival of offspring, in which epigenetic information transmission from parents to offspring plays a prominent role [4, 5]. The gametes, derived from germline cells, act as vehicles through which epigenetic information is passed from one generation to the next [5–7]. Simultaneously, maintaining the integrity of a parent's epigenetic information in the face of environmental challenges, and ensuring its precise transmission, is critical for the progeny. Yet, the detailed workings of this process and the fundamental molecular mechanisms involved still largely remain a mystery. Even though resetting of

Received: June 26, 2024. **Revised:** January 14, 2025. **Editorial Decision:** February 6, 2025. **Accepted:** February 10, 2025

the germline could help erase the epigenetic markers of genes [8–10], some epigenetic responses triggered by the environment can still be passed on [11–16], emphasizing that maintaining the integrity of a parent's epigenetic information is crucial. During the reproductive period, an organism's gametogenesis is particularly vulnerable to heat stress through epigenetic processes [17]. Heat-stress-induced epigenetic changes can be inherited through the germline for multiple generations [18–20]. Paternal germline chromatin is especially threatened by heat stress in pachytene spermatocytes [21, 22], where heat shock proteins do not respond to HSF1 [21].

Argonaute proteins serve as key regulators within all RNAi-related small RNA pathways, where they, along with their associated small guide RNAs (19–35 nucleotides), assemble into RNA-induced silencing complexes. These complexes are adept at modulating the expression of complementary transcripts, either at the transcriptional or post-transcriptional level [23, 24]. In the defense against RNA viruses, the RNA interference (RNAi) pathway orchestrates the epigenetic silencing of viral transcripts [25–28]. During periods of starvation, the Argonaute protein HRDE-1, together with small RNAs, can influence the expression of genes related to nutrition across generations [29, 30]. Collectively, these studies indicate that Argonaute/small RNA pathways play a role in epigenetically modulating gene expression, which assists offspring in adapting to environmental stresses. However, it remains poorly understood whether Argonaute proteins contribute to the preservation of epigenetic information under environmental stress, facilitates the precise transfer of such information to offspring, and subsequently aids in the survival of the progeny.

Among the 21 Argonaute proteins in *Caenorhabditis elegans* [31], CSR-1 is essential and exists in two isoforms: CSR-1A and CSR-1B. CSR-1B performs multiple biological functions [32–37], and mutations in this isoform cause embryonic lethality. CSR-1A is expressed in sperm cells associated with 22G-RNAs that map to spermatogenesis-specific genes and in some somatic cells, such as the intestine and spermatheca [38, 39]. *C. elegans*, with its hermaphrodite and male forms, is an ideal model for studying developmental biology. The major male mating structures include the blunt tail with fan and rays, the hook, the spicules, the proctodeum, and the thin body [40–42]. These unique structures help differentiate males from hermaphrodites during larval development [40, 41] and assist in male mating. During the cross-ability assay (seen in the "Materials and method" section), we collected a cohort of *csr-1a* mutant males derived through conventional heat stress induction [43, 44]. Intriguingly, L4 stage *csr-1a* mutant hermaphrodites exposed to heat stress produced male offspring with abnormal tails. Here, we report that in response to heat stress, Argonaute CSR-1A potentiates the steadiness of sperm-inherited H3K9me3 bookmarking (an epigenetic mechanism of gene expression transmission through generations) and protects tail anatomical structure development of male offspring by suppressing the post-embryonic overexpression of disorganized muscle protein DIM-1.

Materials and methods

C. elegans strains

C. elegans used in this study are listed in Supplementary Table S1.

Growth conditions of *C. elegans* strains

All *C. elegans* strains were grown and maintained at a temperature of 15°C under standard conditions. The specific temperatures used for individual experiments are indicated in the corresponding figures. The *C. elegans* were fed with *Escherichia coli* OP50, which was obtained from the Caenorhabditis Genetics Center. *Escherhabia coli* OP50 was seeded onto the culture plates 3 days before use.

Generation of CRISPR strains

The generation of *C. elegans* strains (seen in Supplementary Table S1) was done using previously described CRISPR-Cas9 ribonucleoprotein (RNP) methods [45]. This process involved co-injecting 0.5 μl (5 μg) of Cas9 protein with 0.4 μg/μl sgRNA (transcribed via T7 RNA polymerase from a DNA template) to form Cas9 RNPs, 2 μg of donors (including oligonucleotides or melted PCR products) (Supplementary Table S2), and either a 50 ng/μl *rol-6* or 20 ng/μl *myo-2::gfp* marker for easy identification of transformed *C. elegans*. To ensure genetic diversity and to test for off-target effects, at least two independent alleles were generated for each strain. This was done by adding different tags or inducing mutations at endogenous loci, thereby manipulating the genome to create genetically modified organisms for further study. CRISPR strains were outcrossed twice before use.

Generation of extrachromosomal array strains

The generation of Extrachromosomal array strains was modified from [46]. For construction of the Plasmid Donor: the plasmid donor was created with a 500 base pair promoter and a 500 base pair 3′Untranslated Region (UTR) of the genes of interest. For injection: a mixture of 100 ng of the plasmid donor and 50 ng of the *rol-6* marker (used to identify transformed organisms) in a 1:1 ratio were co-injected into the germline of *C. elegans*.

For culturing: worms with the desired arrays or roller phenotypes were identified and cultured for 2–3 generations. For selection: 100 L4 stage worms containing the arrays of interest were moved to an empty plate. For irradiation, ∼500 μL of 1X M9 buffer, supplemented with 30 μg/mL TMP (Trimethoprim; catalog no. AC229881000, Thermo Fisher Scientific), was spread on the plate to allow the worms to soak in it for 15 min. The worms were then irradiated using a Stratalinker (Jena) at 250 joules/m^2 with the plate lid removed. For transfer and culture: the worms were then transferred to four or five regular OP50 plates and cultivated until they consumed all the food (∼2 days at room temperature). For chunking and screening: the plates were chunked (i.e. a small portion of the plate was transferred) to a new plate, and 500 worms were singled out per plate to determine if they were integrants in the next generation. Successful integrants should show 100% of progeny containing the co-injection marker.

Heat-stress assay

Heat-stress experiments were modified according to the protocol by [44]. Briefly, Bleached-hatched L1 worms were seeded on 60 mm NGM plates and cultured at 15°C. Late L4 stage worms were transferred to a 37°C incubator (Bluebird) for 1 h. Following heat exposure, the worms were allowed to recover overnight in a 15°C incubator. Healthy and energetic

worms were then selected and placed on 35 mm NGM plates (four worms per plate) and cultured at 15°C. Additional heat exposure experiments were conducted at 28°C and 33°C for 1 h. The worms were allowed to develop into young adults, and males were subsequently picked and their tail morphology was observed. The total number of males and males with abnormal tail morphology were counted. The specific heat-stress temperatures and the developmental stages of the worms used for each experiment are indicated in the corresponding figures. For heat-stress analysis of L1/L2 and L3 worms, worms were mated for two to three generations to maintain about 10–20% male progeny per generation.

Maternal or paternal transmission assay

Males and hermaphrodites (*unc-119*) in the *gfp::tev::2* × *flag::aid::csr-1a* and *gfp::tev::2* × *flag::aid::csr-1a*△ strains were isolated at the young adult and L4 developmental stages, respectively. The isolated males or hermaphrodites (*unc-119*) were exposed to heat shock (37°C, 1 h), then allowed to recover for a while. Heat-stressed males were mated with non-heat-stressed hermaphrodites (*unc-119*), and heat-stressed hermaphrodites were mated with non-heat-stressed males. Mating was conducted for 24 h at 15°C. Mated hermaphrodites (*unc-119*) were then singled per plate, and their male progenies that could move freely were picked at the young adult stage. The tail morphology of these progenies was observed. The total numbers of males and males with abnormal tail morphology were counted. The number of males mating with hermaphrodites was maintained at a 4:1 ratio, and 400 mating plates for each group per repeat were required to produce enough male-crossed progeny.

Paternal transmission assay (crossing at different time points post-heat stress)

This protocol is a modification of the one described by [47] and involves assessing the impact of heat shock on male paternal transmission.

Worm Preparation: Worms were mated for two to three generations to maintain about 10–20% male progeny per generation. Thousands of young adult male worms were isolated for the experiment.

Post-Heat Stress Crossings: Following heat stress (37°C, 1 h), four males were paired with one non-heat stressed hermaphrodite (*unc-119*) at various time points post-heat stress. The specific time intervals of pairing post-heat stress were: 0–4 h, 4–8 h, 8–10 h, 10–12 h, 12–14 h, 14–16 h, and 16–24 h. For each time interval, before pairing with the non-heat-stressed hermaphrodites (*unc-119*), males were first mated with a *wild-type* hermaphrodite for the corresponding number of hours in order to purge sperm that were generated prior to heat stress. After each cross, hermaphrodites (*unc-119*) were immediately singled out to produce progeny.

Strain Specific Crossings: For different strains, gfp::tev::2 × flag::aid::csr-1a (ezs435) males were crossed with gfp::tev::2 × flag::aid::csr-1a;unc-119 hermaphrodites (ezs438) and gfp::tev::2 × flag::aid::csr-1a△ (ezs436) males were crossed with gfp::tev::2 × flag::aid::csr-1a△; unc-119 (ezs439) hermaphrodites.

Worm Selection: Crossed males that could move freely were picked until worms developed into young adults.

Observation and Counting: The tail morphology of the young adults was observed, and the total numbers of males and males with abnormal tail morphology were counted.

Number of Plates: A total of 800 mating plates for each group per repeat were needed to produce enough male-crossed progeny.

Cross ability assay

Young adult males were isolated after their parents were subjected to heat stress (37°C, 1 h) at the late L4 stage. Four Males were mated with one hermaphrodite (*unc-119*) for 24 h in 15°C. Crossed males that could move freely were picked until worms developed into young adults and numbers of total crossed males were counted. The number of males for each strain that was used to mate with hermaphrodites (*unc-119*) was comparable.

Sperm activation assay

After their parents were subjected to heat stress at the late L4 stage, young adult males were picked and placed on an NGM plate without seeding on OP50 plates before the assay. Approximately 6–7 males were dissected in 10 μl of sperm medium (50 mM HEPES, 50 mM NaCl, 25 mM KCl, 5 mM CaCl2, 1 mM MgSO4) containing 200 μg/mL Pronase E (catalog no. P8811, Sigma). Round spermatids were incubated for 15 min at room temperature in a humid chamber prior to mounting. Specimens were mounted and imaged on a microscope (ZEISS) using a 60x N.A. 1.42 oil-immersion objective. The numbers of spermatozoa that were successfully induced from round spermatids, sperm that were partially activated or had short spikes, and sperm that were not activated (round spermatids) were counted.

Life span assay

Worms hatched from bleach-treated eggs, whose parents were subjected to heat stress at the late L4 stage, were cultivated until they reached the L4 stage. Males were picked and transferred to new plates every 2 days. The male worms were cultivated at a temperature of 15°C. The total number of alive males was counted every two days.

Tissue-specific auxin-mediated protein degradation in *C. elegans*

OP50 clones were grown overnight in LB liquid culture, then added with IAA (500 uM, catalog no. A10556, ThermoFisher) for 2 h before seeding the bacteria (10X) on NGM plates supplemented with IAA (500 mg/ml). Bleach-hatched L1 worms were dispersed onto IAA-NGM plates. This was done with or without the parental late L4 heat stress. The worms were cultured on IAA-NGM plates until they reached the L3 stage. They were then transferred to OP50 plates and washed several times with 1X M9 buffer. The tail morphology of the worms was observed. The total numbers of males and males with abnormal tail morphology were counted.

RNA interference screening

RNAi was performed by feeding bacteria expressing dsRNA targeting the gene of interest. RNAi feeding clones were selected from the ORFeome RNAi library, which is available from the MRC [48]. Bacterial clones expressing the control (empty vector pL4440) construct and the dsRNA targeting

different *C. elegans* genes were obtained from *C. elegans* ORFeome [48], which contains up to 11 942 cloned protein-encoding open reading frames (ORFs) [48]. The plasmids were generated by the Gateway recombinational cloning of all predicted protein-encoding ORFs of *C. elegans* and were kept in *E. coli*. All RNAi clones used in experiments were sequenced for verification before use. For RNAi experiments, RNAi bacteria with empty (pL4440 vector as control) or the dsRNA-expressing plasmid were grown overnight in liquid LB media containing ampicillin (100 mg/ml) and then induced with IPTG (1 mM, catalog no. 0487, AMRESCO) for 2 h before seeding the bacteria (10X) on NGM plates supplemented with ampicillin (100 mg/ml, catalog no. A610028, Sangon Biotech), and IPTG (1 mM). Bleach-hatched L1 worms were dispersed onto RNAi plates. This was done with or without subjecting the parental worms to late L4 stage heat stress. Tail morphology was observed. The total numbers of males and males with abnormal tail morphology were counted.

Isolation of germline cells

This protocol, adapted from reference [49], outlines the isolation of germline cells from bleach-hatched worms. Approximately 30 million bleach-hatched worms from each strain were grown to the late L4 stage and harvested into 15 ml conical tubes using 1 × M9 buffer. The worms underwent more than 10 washes with 1 × M9 buffer, followed by three washes with water. They were then transferred to a 1.5 ml microcentrifuge tube, and centrifuged at 16 000 rpm for 2 min, reducing the volume to 80 µl of packed worms by discarding excess water. Next, 200 µl of freshly thawed SDS-DTT was added, and the mixture was incubated for exactly 4 min at 25°C in a shaking incubator set to 1200 rpm. After SDS-DTT treatment (200 mM DTT, 0.25% SDS, 20 mM HEPES, pH 8.0, 3% sucrose), the reaction was halted by adding 800 µl of egg buffer (118 mM NaCl, 48 mM KCl, 2 mM CaCl2, 2 mM MgCl2, 25 mM HEPES, pH 7.3, osmolarity 340 mOsm). The lysates were washed five additional times with 1 ml of egg buffer. Each tube then received 100 µl of freshly thawed 15 mg/ml pronase E (catalog no. P8811, Sigma) and was incubated at 25°C for 30 min in a shaking incubator set to 1200 rpm. The reaction was stopped by adding 900 µl of egg-buffer/FBS (10%). The digested larvae were centrifuged at 9600 × g for 5 min at 4°C and washed twice more with 1 ml of egg-buffer/FBS. The digested lysates were resuspended in egg-buffer/FBS and filtered through a 45 µm cell strainer. These samples were enriched using a Percoll gradient and analyzed with a cell sorter (cytoFLEX SRT -1, Beckman Coulter). GFP marker strains (*gfp::tev::2* × *flag::aid::csr-1a* (*ezs435)* and *gfp::sl2::2* × *flag::aid::csr-1a*△ (*ezs458)*) and N2 profiles were used for gating to analyze CSR-1A-expressing germ cells. Data analysis was performed using FlowJo software.

Dissection and purification of *C. elegans* round spermatids

The protocol for dissection and purification of *C. elegans* round spermatids was modified by Dr. Tang's lab [50]. Young adult male worms were initially subjected to heat stress at 37°C for 1 h and then allowed to recover at 15°C. After 8–10 h, the worms were immediately dissected to release round spermatids. The released materials were incubated in L-15 medium (catalog no. 21083–027, Gibco), supplemented with 15% FBS (catalog no. 10270–106, Gibco) and 1% sucrose. These samples were subsequently analyzed using a MoFlo Astrios cell sorter (Beckman Coulter) equipped with Moflo Summit 6.3.1. The size range of the samples was estimated by comparing the forward scatter signals with those from reference microspheres (The Flow Cytometry Submicron Particle Size Reference Kit, Thermo Fisher). This size information was used for gating to analyze mitophers and spermatids. FlowJo software was employed for data analysis. After collecting pure sperm, they were washed twice with 1X phosphate-buffered saline (PBS) for further analysis.

Immunostaining of dissected worms

Immunostaining of dissected worms was performed according to previously published protocol by [18]. After heat stress, male worms were washed with 1X M9 buffer and then dissected near their heads using a blade to release the germline. The germline was immediately fixed in freshly prepared 4% paraformaldehyde (catalog no. FB24243, FEIMOBIO) and left to incubate overnight at 4°C. The fixed germline was washed with 1 × phosphate-buffered saline with 0.1% Tween detergent (1 × PBST). Cold methanol was added to the germline and left at −20°C for 4 h. The germline was again washed with 1 × PBST. The germline was then blocked in 1 × PBST supplemented with 5% BSA for 1 h. The germline was stained overnight at 4°C with Hoechst 33 342 (1:10 000, catalog no. A9539, Sigma) and rabbit anti-H3K9me3 antibody (1:200, catalog no. ab8898, Abcam), both diluted in 1 × PBST. The next day, the germline was rinsed in 1 × PBST and incubated with Alexa Fluor 594 goat anti-rabbit IgG (H + L) antibody (1:400, catalog no. A-11012, ThermoFisher Scientific) for 4 h at room temperature. The germline was then washed with 1 × PBST. Post-washing, the germline was mounted on slides. A spinning disk confocal microscope (Leica) equipped with a 60 × oil objective was used to capture images. The images were obtained and processed using Imaris software. Fluorescence of the germline labeled by H3K9me3 was quantified using Imaris software. The threshold setting was adjusted to yield a similar low reading for the control of each experiment.

Immunostaining of worms

For worm staining, worms were washed with 1X M9 buffer and fixed with freshly prepared 4% paraformaldehyde overnight at 4°C. After washing with 1 × PBST, the specimens were treated with cold methanol was added and stored at −20°C for 4 h. The fixed worms were rewashed with 1 × PBST, stained with Hoechst 33 342 (1:10 000), and left overnight at 4°C. A spinning disk Confocal Microscope (Leica) with a 60 × oil objective was used for visualization. 3D images were captured to evaluate the volume of rectal valve and rectal gland cells (RVRG). Image acquisition and processing were conducted using Imaris software. This software was also employed to quantify the volume of RVRG cells, with the threshold setting adjusted to yield a similar low reading for the control of each experiment.

Propidium iodide staining of worms with RP defect

Male worms were picked in 1XM9 buffer with propidium iodide (1:10 000, catalog no. P1304MP, Thermo) and stained for 15 min. A spinning disk Confocal Microscope (Leica) with a 60 × oil objective was used to ascertain whether RP defect cells were stained with propidium iodide, a marker indicat-

ing the vitality or mortality of RP defect cells. A male worm, fixed with 4% paraformaldehyde stained with propidium iodide, served as a positive control.

Imaging of live worms

For observing RVRGs development along with RP defect formation: After parental late L4 heat stress, bleach-hatched worms were cultured until L3 at 15°C. A male worm was carefully selected and placed on slides in 1XM9 buffer with 10 μM tetramisole hydrochloride (catalog no. L9756, Sigma) to induce temporary paralysis. A 3D imaging of RVRG cells was performed, marked by Ppcs-1::wrmScarlet and Ppnc-1::wrmScarlet. The worm was then carefully transferred back to the plate within a few minutes. As the worm grew to middle L4, late L4, or young adult stages, the imaging steps were repeated. Imaris software was used to obtain, process, and quantify the volume of RVRG cells, marked by Ppcs-1::wrmScarlet and Ppnc-1::wrmScarlet. The threshold setting was adjusted to yield a similar low reading for each experiment's control.

For observation of DIM-1::wrmScarlet expression in L1 hermaphrodite or male worms: Worms were mated for two to three generations to maintain approximately 10 to 20 percent male progeny per generation. An L1 worm was picked carefully and placed on slides in M9 buffer containing 10 μM tetramisole hydrochloride (catalog no. L9756, Sigma) for temporary paralysis. This enabled the imaging of the RVRG cells marked by DIM-1::wrmScarlet. Each worm was then individually transferred to a separate plate. As it matured to the young adult stage, its sex and tail morphology were recorded. Approximately 200 L1 worms were needed to observe DIM-1::wrmScarlet expression in L1 male worms with RP defects.

Imaging of germ cells post heat stress

Cells were isolated and centrifuged at 9600 x g at 4°C for 5 min. The supernatants were cautiously discarded, leaving behind 10–15 μl to re-suspend the cells. These cells were subsequently stained with propidium iodide (1:10 000 dilution, catalog no. P1304MP, Thermo) to assess their viability. The cells were incubated at 37°C in a water bath for 15 min or were then incubated at 37°C in a water bath for 15 min before being swiftly transferred to RT for 60 min. Following this, they were mounted onto slides. Cells that were not subjected to heat stress served as a control group. Imaging was carried out using a spinning disk confocal microscope (Leica) with a 60X oil immersion objective lens.

Western blot analysis of round spermatids in worms

Thousands of young adult male worms were collected on an NGM plate and subjected to heat stress at 37°C for 1 h. Following this, the males were transferred to a 15°C environment to recover for approximately 10 h. The worms were then dissected to isolate round spermatids. The released material was incubated in L-15 medium (catalog no. 21083–027, Gibco) containing 15% FBS (catalog no. 10270–106, Gibco), and 1% sucrose [50]. After FACS sorting, pure round spermatids were collected using a micropipette, washed twice with 1 × PBS, vortexed briefly with the SDS loading buffer, and heated at 95°C for 10 min. The lysates were separated on 4–12% Bis-Tris polyacrylamide gels and transferred to PVDF membranes. The membranes were probed with the following primary antibodies overnight: rabbit anti-H3K9me3 (1:1000, catalog no. ab8898, abcam), rabbit anti-H3K4me2 (1:1000, catalog no. ab272142, abcam), rabbit anti-H3K27me3 (1:2000, catalog no. C36B11, Cell Signaling), rabbit anti-H3K36me3 (1:2000, catalog no. ab9050, abcam), mouse anti-H3K9me2 (1:2000, catalog no. ab1220, abcam), and rabbit anti-Histone H3 (1:1000, catalog no. Ab18521, abcam). Secondary antibodies (goat anti-rabbit IgG (H + L) anti-body (1:2000, catalog no. RS001, Immunology), goat anti-mouse IgG (H + L) antibody (1:2000, catalog no. RS002, Immunology) were then incubated for 1 h. Protein expression, normalized to Histone H3 levels, was measured across different samples using ImageJ. Around 100 000 round spermatids were required to generate one sample.

Western blot analysis of germline cells

Isolated cells were centrifuged at 9600 x g at 4°C for 5 min. Supernatants were carefully removed, leaving behind 10–15 μl to re-suspend the cells. The cells were then incubated at 37°C in a water bath for 15 min and immediately transferred to RT. At 0, 5, 10, 15, 30, and 60 min of post heat shock, cells were promptly treated with 500 μl RIPA lysis buffer (10 mM Tris-HCl, pH 8.0; 1 mM EDTA; 0.5 mM EGTA; 1% Triton X-100; 0.1% Sodium Deoxycholate; 0.1% SDS; and 140 mM NaCl) for 10 min on ice. The cells were then mixed with SDS loading buffer and heated at 95°C for 10 min. Lysates were separated on 4–12% Bis-Tris polyacrylamide gels, transferred to PVDF membranes, and probed overnight with rabbit anti-H3K9me3 antibody (1:1000, catalog no. ab8898, abcam) and rabbit anti-Histone H3 antibody (1:1000, catalog no. Ab18521, abcam). Goat anti-rabbit IgG (H + L) secondary antibody (1:2000, catalog no. RS001, Immunology) was incubated for 1 h. Protein expression was measured across different samples using ImageJ. Quantified H3K9me3 levels were normalized to their respective Histone H3 levels (loading control). Approximately 100 000 germline cells were required to generate one sample.

Western blot analysis of worms

Bleach-hatched worms were cultivated at 20°C and harvested after 2 h (L1 stage), 32 h (L3 stage), 46 h (L4 stage), and 72 h (gravid adult stage) post-cultivation on OP50. Worm pellets were prepared with 1 ml of L1, 500 μl of L3, 50 μl of L4, and 30 μl of gravid adults. Each sample was mixed with 4 × Laemmli sample buffer, supplemented with 5% beta-mercaptoethanol, and then boiled for 30 min with occasional flipping every 5 min. Whole-worm lysates were separated on 4–12% Bis-Tris polyacrylamide gels, transferred to PVDF membranes, and probed overnight with the following primary antibodies: mouse anti-FLAG M2 (1:1000, catalog no. F1804, Thermo), mouse anti-alpha tubulin (1:4000, catalog no. T9026, Sigma), or mouse anti-V5 antibodies (1:2000, catalog no. R96025, Thermo). The membranes were then incubated for 1 h with a secondary antibody, goat anti-mouse IgG (H + L) (1:2000, catalog no. RS002, Immunology). Protein expression, relative to alpha-tubulin levels, was measured across different samples using ImageJ.

Co-immunoprecipitation and western blotting

Around 300 000 late L4 worms per condition (non-heat stressed control or heat stressed at 37°C for 1 h) were immediately cross-linked using UV, collected in 1 × M9 buffer, washed with water, and snap-frozen in liquid nitrogen. Worm

pellets were resuspended in an equal volume of pre-chilled 1 x lysis buffer (60 mM HEPES (pH7.4), 100 mM KCl, 4 mM MgCl2, 10% Triton X-100, 10% Tween-20, supplemented with 1 mM DTT and a protease inhibitor cocktail) along with 200 μl glass beads. The samples were homogenized and then centrifuged at 15 000 rpm for 30 min at 4°C to remove worm debris. 10% of the worm lysates were set aside as input. The remaining lysates were incubated with mouse anti-FLAG M2 antibody (1:400, catalog no. F1804, Thermo) or mouse anti-V5 antibodies (1:400, catalog no. R96025, Thermo) overnight, followed by a 4-h incubation with magnetic protein G beads (1:200; catalog no. 10004D, Invitrogen). The beads were pre-cleared with pre-chilled 1 × lysis buffer prior to incubation. *Wild-type* (N2) worms were used as a negative control. If necessary, lysates were pre-treated with RNase A. The immunoprecipitates were boiled with 4X SDS sample buffer (BioRad), separated by SDS-PAGE, and transferred to PVDF membranes. The blots were probed with mouse anti-FLAG M2 antibody (1:1000, catalog no. F1804, Thermo), mouse anti-alpha tubulin antibody (1:4000, catalog no. T9026, Sigma), or mouse anti-V5 antibodies (1:2000, catalog no. R96025, Thermo).

Nuclear/cytoplasmic fractionation of proteins

The method for nuclear/cytoplasmic fractionation of proteins was partially adapted from referenced literature [51]. Synchronized late L4 worms were treated in a 37°C incubator for 1 h and then collected with M9 buffer in a 15 ml conical tube. The worm pellets were washed with M9 buffer until the supernatant was clear. They were then washed twice with cold hypotonic buffer (15 mM HEPES KOH pH 7.6, 10 mM KCl, 5 mM MgCl2, 0.1 mM EDTA, 350 mM Sucrose) in a 1.5 ml tube. All hypotonic buffer was removed and replaced with 'complete hypotonic buffer' (15 mM HEPES KOH pH 7.6, 10 mM KCl, 5 mM MgCl2, 0.1 mM EDTA, 350 mM Sucrose, 1 mM DTT, 2x protease inhibitors). The worm pellets were then resuspended and homogenized by 6.5 m/s for 30 cycles, repeated 5–10 times. Worm bodies and debris were removed by centrifugation at 500 x g for 5 min at 4°C, twice. A 40μl aliquot of the supernatant was saved for the input fraction. The remaining supernatant was centrifuged at 4000 x g in 4°C for 5 min to pellet the nuclei. The supernatant was thereafter transferred to a new 1.5 ml tube and then centrifuged at 17 000 x g, 4°C for 30 min to collect the cytoplasmic fraction. The pellet, which contains nuclei, was washed with 500 μl complete hypotonic buffer and centrifuged at 4000 x g in 4°C for 5 min, twice. The supernatant was discarded, and the pellet was dissolved with complete hypertonic buffer (15 mM HEPES KOH pH 7.6, 400 mM KCl, 5 mM MgCl2, 0.1 mM EDTA, 0.1% Tween 20, 10% Glycerol, 1 mM DTT, 2x protease inhibitors). The cytoplasmic fraction and nuclear fraction were then incubated with mouse anti-V5 antibodies (1:400, catalog no. R96025, Thermo) or anti-mouse IgG (1:400, catalog no. M8642, Thermo) for the co-immunoprecipitation assay.

Worm chromatin immunoprecipitation (ChIP) PCR

The Chromatin immunoprecipitation (ChIP) protocol was modified according to previously published methods [18]. Approximately 30 μl of worm pellets of late L4 animals were obtained via the 'bleach-hatch' method. Immediately after heat shock at 37°C for 1 h, animals were quickly washed with 1 × PBS (pH 7.4). Cross-linking was performed with freshly prepared 2% formaldehyde at room temperature for 10 min. A typical volume of 1 mL of formaldehyde was used to ensure consistency across samples. To quench the samples, Tris (pH 7.4) was added to a final concentration of 250 mM, and the samples were left at room temperature for 10 min. The samples were then washed three times in ice-cold 1 × PBS supplemented with a protease inhibitor cocktail and snap-frozen in liquid nitrogen. The worm pellet was resuspended in FA buffer [50 mM HEPES (pH7.4), 150 mM NaCl, 50 mM EDTA, 1% Triton X-100, 0.5% SDS, and 0.1% sodium deoxycholate], supplemented with 1 mM DTT and protease inhibitor cocktail. Following the addition of FA buffer, the suspended worm pellet was lysed using a homogenizer supplemented with 100 μl glass beads (6.5 m/s, 30 s once) and then sonicated (15 cycles of 30 s on/off). Samples were centrifuged at 11 731 x g for 5 min at 4°C to remove worm debris. Around 20 μl of lysate was used to preclear magnetic beads. Lysates were incubated with mouse anti-FLAG M2 antibody (1:400, catalog no. F1804, Thermo) or mouse anti-V5 antibodies (1:400, catalog no. R96025, Thermo) overnight and then incubated with magnetic protein G beads (1:200; catalog no. 10004D, Invitrogen) for 4 h. Anti-mouse IgG antibody was used as a negative control. Beads were washed with low salt, high salt, and LiCl wash buffers for 5 min at 4°C. Protein complexes were eluted by incubation with 250 μl of freshly prepared elution buffer (1% SDS and 100 mM sodium bicarbonate) for 15 min at room temperature. Elutes were treated with Proteinase K solution (1:10, catalog no. P8107S, NEB) for 30 min, incubated with RNase A (1:10, catalog no. T3018L, NEB) for 2 h, and extracted with phenol:chloroform:isoamyl alcohol (25:24:1). After ethanol precipitation, DNA was extracted. qPCR analysis of DNA was performed using primer sets specific for different target genes. For all ChIP experiments, 10% of total lysate was used as 'input', and chromatin immunoprecipitated by different antibodies was expressed as % input values. All relative changes were normalized to *Y43F4A.3*. Fold changes were calculated by the $^{\triangle\triangle}$Ct method.

Round spermatids and germ cells chromatin immunoprecipitation (ChIP-PCR)

For germ cells, approximately 300 000 isolated germ cells per condition were centrifuged at 9600 x g at 4°C for 5 min. Supernatants were carefully removed, leaving 10–15 μl supernatant to resolve the cells. Cells were incubated at 37°C in a water bath for 15 min and immediately transferred to RT. After 0, 5, 10, 15, 30, and 60 min of post heat shock, cells were immediately incubated with 100 μl pre-chilled NE buffer, resuspended by gentle pipetting, and incubated on ice for 10 min. For round spermatids, approximately 300 000 round spermatids and 30 293-F cells (as spike-in) per condition were prepared for sperm ChIP-PCR based on the Hyperactive® Universal CUT&Tag Assay Kit for Illumina (catalog no.TD903, Vazyme). Round spermatids were washed twice in 500 μl Wash Buffer by gentle pipetting, and centrifuged for 5 min at 1700 × g. Each sample was added 100 μl pre-chilled NE buffer, resuspended by gentle pipetting, and incubated on ice for 10 min. The nucleus of germ cells and round spermatids were then processed following the protocol of the Hyperactive pG-MNase CUT&RUN Assay Kit for PCR/qPCR (catalog no. HD101, Vazyme). qPCR analysis of DNA was performed using primer sets specific for different target genes. Around

10% of total lysate was used as 'input', and chromatin immunoprecipitated by different antibodies was expressed as % input values. For round spermatids, all relative changes were normalized to *Y43F4A.3*. For germ cells, all relative changes were normalized to individual gene at 0 min of post heat-stress in *gfp::tev::2* × *flag::aid::csr-1a* group. Fold changes were calculated by the $^{\triangle\triangle}$Ct method.

Isolation of rectal gland and valve cells

Parental late L4 worms underwent heat stress (37°C, 1 h), and 2 million synchronized L1 worms in each strain were cultured until adulthood. The mixture of gravid hermaphrodites and adult males (day 1 adults) was collected. Worms were suspended with an equal volume of 60% ice-cold sucrose and centrifuged for 5 min at 1000 xg. Worms in the top layer were collected on 20-micron Nytex mesh and rinsed with S-basal (5.85 g NaCl, 1 g K_2HPO_4, 6 g KH_2PO_4, 1 ml cholesterol (5 mg/ml in ethanol)). Males were allowed to wiggle through the mesh for at least 30 min [7]. Worms were washed with M9 for 1 h to flush bacteria out of the nematodes' gut. Every 200 µl pellet of them was transferred to a 1.5 mL microcentrifuge tube and centrifuged at 16 000 x g for 1 min. The pellets were then treated with 500 µL of freshly made Triton X-100/SDS-DTT solution (0.5% Triton X-100,20 mM HEPES buffer, pH 8, 0.25% SDS, 200 mM DTT, and 3% sucrose) and incubated at room temperature at 1300 rpm for 4 min. Immediately after that, 800µL of egg buffer (25 mM HEPES, pH 7.3, 118 mM NaCl, 48 mM KCl, 2 mM $CaCl_2$, 2 mM $MgCl_2$) was added to each tube and centrifuged for 1 min at 16 000 x g. The supernatant was discarded, and the pellet was washed five times with 1 mL of egg buffer. Around 1 ml of freshly made 15 mg/ml pronase (catalog no. P8811, Sigma) was added to the tubes and each sample was pipetted 40–80 times with a P1000 pipette at 3–4-min intervals during the digestion. The enzymatic reaction was stopped by adding egg-buffer/10% FBS and the isolated cells were centrifuged at 4°C for 5 min at 550 x g. The pellet was resuspended in 1 mL of cold egg buffer/10% FBS and centrifuged at 4°C for 5 min at 100 x g. The supernatant was then passed through a 35-µm filter (catalog no. 352 235, Corning). The cell suspensions were sorted by SONY MA900. Profiles of GFP and wrmScarlet marker strains were compared to an N2 standard to exclude autofluorescent cells. 5000 positive cells were collected in TRIzol reagent (catalog no. T9424, Sigma) for total RNA extraction. RNA was precipitated from the aqueous phase by mixing with isopropyl alcohol.

mRNA sequencing

mRNA libraries were prepared using the VAHTS Universal V8 RNA-seq Library Prep Kit for Illumina (catalog no.NR605, Vazyme). This kit is designed to construct libraries for sequencing on Illumina platforms. Once the libraries were prepared, they underwent quality assessment using an Agilent 2100 Bioanalyzer System (High Sensitivity DNA Analysis kit). Finally, the prepared and evaluated libraries were sequenced on an Illumina HiSeq2500 platform.

CUT&Tag analysis for *C. elegans* round spermatids

Approximately 300 000 round spermatids per sample were prepared for CUT&Tag. The process was performed following the protocol provided by the Hyperactive Universal CUT&Tag Assay Kit for Illumina Pro (catalog no. TD904, Vazyme). Thirty of 293-F cells were added as a spike-in. The sperm were washed twice in 1.5 mL of Wash Buffer by gentle pipetting and then centrifuged for 5 min at 1700 × g. To each sample, 100 µl of pre-chilled NE buffer was added, and the samples were gently resuspended by pipetting up and down. The samples were then incubated on ice for 10 min. The nuclei were processed following the protocol of the Hyperactive Universal CUT&Tag Assay Kit for Illumina Pro (catalog no. TD904, Vazyme). Once the libraries were prepared, they were evaluated using the Agilent 2100 Bioanalyzer System.

Analysis of mRNA-seq data

For pre-processing: adapters and low-quality bases were removed from the raw sequencing reads using the tool fastp (version 0.20.1) (options: -q 20 -n 0 -u 50 -l 75 -c). For mapping: the trimmed reads were then mapped to the reference genome (*C. elegans* genome WS276) using the Spliced Transcripts Alignment to a Reference (STAR) software (version 2.5.2b). The options applied (–outSAMunmapped Within –outSAMstrandField intronMotif –outFilterMultimapNmax 1 –outFilterScoreMinOverLread 0.8 –outFilterMatchNminOverLread 0.8). For counting: read counts per gene were calculated using featureCounts, a function of the Subread package (version 2.0.0). For differential Expression Analysis, the read count data were then used for differential gene expression analysis using the DESeq2 R package.

CUT&Tag data analysis

The following protocol outlines the approach to the analysis of CUT&Tag data, modified from the protocol in Ye Zheng's lab [52].

Pre-processing: adapters and low-quality bases were removed from the raw sequencing reads using the tool fastp (version 0.20.1) (options: -q 20 -n 0 -u 50 -l 75 -c).

Mapping: the trimmed reads were mapped to the *C. elegans* genome (WS276) using Bowtie2 (version 2.3.5.1). The options applied (–end-to-end –very-sensitive –no-mixed –no-discordant –phred33 -I 10 -X 700) control parameters such as the alignment mode, sensitivity, and insert size. For spike-in calibration, the trimmed reads were additionally mapped to the human genome (GRCh38).

Spike-in Calibration: The mapped files were calibrated using the calculated scale factors and converted to genomic coverage bedgraph files using the bedtools genomecov function.

Visualization: Normalized bedgraph files were converted to BigWig files using UCSC bedGraphToBigWig. Biological replicates in BigWig files were merged using UCSC BigWigMerge. The density of genome features in each chromosome was calculated with UCSC BigWigSummary from BigWig files. The genome browser views were generated by visualizing the BigWig files in the Integrative Genomics Viewer (IGV).

Read Counts: Read counts were obtained using an R script and normalized to human map reads per million.

Differential Expression Analysis: Differential gene expression analysis was performed using an R script. The significance of differential expression (*P*-value) was calculated using the Student's *t*-test.

Quantification and statistical analysis

Each experiment was treated as a biological replicate. Specific statistical details for each experiment, including the statistical

tests used and the number of replicates, can be found in the corresponding figure legends. Data analysis was performed using Student's t-test and/or one-way ANOVA with Tukey's correction, utilizing GraphPad Prism software. The significance of the results was determined based on the calculated p-values. The levels of significance are denoted as follows: $*P < 0.05$; $**P < 0.01$; $***P < 0.001$; $****P < 0.0001$.

Results

Transient degradation of germline Argonaute CSR-1A leads to somatic defects in male offspring under heat stress

To investigate the biological function of CSR-1A, we used CRISPR/Cas9 genome editing to endogenously tag CSR-1A at its N-terminus with a GFP::TEV::2XFLAG::AID tag (termed GTFA), resulting in the strain *gtfa::csr-1a (ezs435)* (Supplementary Fig. S1A). We then specifically deleted a single nucleotide shortly after the *csr-1a* start codon to introduce a frameshift mutation that results in an early stop codon in the first exon of *csr-1a*, creating the strain *gtfa::csr-1a△ (ezs436)* (Supplementary Fig. S1A–C). We then reintroduced the deleted nucleotide in *gtfa::csr-1a△ (ezs436)* to restored CSR-1A function in the strain *gtfa::csr-1aR (ezs437)* (Supplementary Fig. S1A–C). Consistent with prior reports [38,39], *csr-1a* mutant worms maintained at 20°C produced normal numbers of viable progeny or sperm activation rates.

During the cross-ability assay (seen in the method section), we collected a cohort of *csr-1a* males derived through heat stress induction. Intriguingly, however, L4 stage *csr-1a* hermaphrodites exposed to heat stress produced male offspring with abnormal tails (Fig. 1A and B). The penetrance of the morphological defect increased with temperature (Fig. 1C). The morphological defect in offspring induced by parental heat stress appears to be a rectal prolapse (RP), which reduces their locomotion and prevents mating (Fig. 1D). Indeed, the impotence of RP *csr-1a* males appears to be physical, as sperm from *csr-1a* males with or without the RP phenotype showed similar levels of activation *in vitro* (Supplementary Fig. S1D and E). Lastly, whereas *wild-type* or non-RP *csr-1a* adult males survived for ∼28 days, RP *csr-1a* adult worms only survived about 8 days (Fig. 1E), indicating that the prolapse is fatal.

To determine if the abnormal morphology is due to the loss of P0 or F1 germline CSR-1A activity or both, we generated knock-in (KI) strains (*gtfa::csr-1a;[Psun-1::tir-1::mRuby::eft 3′utr]chrIV (ezs462)*) expressing GFP::degron::CSR-1A from the endogenous *csr-1a* locus. We then used the auxin-inducible degradation (AID) system [53] to deplete CSR-1A in the germline conditionally. In this system, germline TIR1 protein (*Psun-1::TIR1::mRuby)* mediates potent auxin-dependent depletion of degron-tagged targets. P0 worms during the L4 stage were heat-stressed and the tail morphology of F1 males was analyzed. To determine if the abnormal morphology is due to the loss of P0 germline CSR-1A activity, P0 worms were fed with auxin (IAA), but F1 males were not. To determine if the abnormal morphology is due to the loss of F1 germline CSR-1A activity, P0 worms were not fed with auxin, but F1 males were fed with auxin. We found that the depletion of P0 germline CSR-1A, not that of the F1 germline CSR-1A, leads to morphological abnormalities in the offspring (Fig. 1F and G). These findings suggest that parental germline CSR-1A plays a protective role in preserving offspring morphology.

In the hermaphrodite germline, CSR-1A is only expressed during spermatogenesis, i.e. during the L4 stage [38, 39]. Consistent with this, we only observed RP male tails among the progeny of *csr-1a*-mutant hermaphrodites who were heat-stressed at mid-to-late L4 stage (Supplementary Fig. S1F), suggesting that the RP phenotype is a paternal effect. Indeed, whereas non-stressed *csr-1a* males mated to heat-stressed *csr-1a* hermaphrodites produced no RP male cross progeny, heat-stressed *csr-1a* males mated to non-stressed *csr-1a* hermaphrodites produced RP male progeny (Supplementary Fig. S1G and H).

In males, pachytene germ cells take 8–16 h to differentiate into mature sperm (Fig. 1H) [47, 54]. We therefore heat stressed young adult males and then serially mated them with non-heat-stressed hermaphrodites for brief periods, transferring the males every 2–4 h to unmated *unc-119* hermaphrodites. A small fraction of cross-progeny males with defective tails was produced by crosses from 4 to 8 h after heat shock (Fig. 1I). The fraction of cross-progeny males with the RP phenotype increased dramatically in crosses from 8 to 14 h after heat shock. Together these results suggest that CSR-1A reinforces a paternal temperature-sensitive epigenetic program important for tail development in male offspring.

CSR-1A recruits SET-25/32 to resist H3K9me3 decline by heat stress

Considering that CSR-1A is selectively present in spermatocytes and not in mature sperm [38, 39], in order to understand how CSR-1A contributes to the regulation of male tail development in offspring, we sought to investigate histone modifications, which are also implicated in epigenetic inheritance [55, 56]. To identify histone modifications that act in the CSR-1A pathway to bolster the paternal epigenetic program required for normal male tail structure or function, we used RNAi by feeding to silence histone methyltransferase genes (or combinations) beginning at the L1 stage, exposed L4-staged animals to heat stress, and then examined the morphology of male progeny (Fig. 2A, Supplementary Fig. S2A). We targeted histone methyltransferases associated with active transcription marks, e.g. H3K4me2 [57] and H3K36me3 [58], or repressive marks, e.g. H3K27me3 [59], H3K9me2 [60, 61], and H3K9me3 [62, 63] (Supplementary Fig. S2A). We only observed RP male tails when we silenced the H3K9 trimethyltransferases *set-25* and *set-32* together. The frequency of RP male tails among the progeny of heat-stressed *set-25/32* RNAi hermaphrodites was similar to that observed in the progeny of heat-stressed *csr-1a* hermaphrodites. Moreover, *set-25/32* RNAi did not exacerbate or increase the penetrance of the RP phenotype caused by loss of CSR-1A (Fig. 2B and Supplementary Fig. S2C). These results suggest that CSR-1A and SET-25/32 act in the same pathway to promote the recovery from heat stress.

To explore the relationship between CSR-1A and SET-25/32 and the response to heat stress, we analyzed the levels of histone methylation in *csr-1a* mutant sperm after heat stress. Western blot analyses of various histone modifications revealed a > 50% reduction in H3K9me3 in heat-stressed sperm from *csr-1a* males compared to that in heat-stressed wild-type sperm (Fig. 2C). H3K4me2, H3K27me3, H3K36me3, H3K9me2, and histone H3 levels appeared normal.

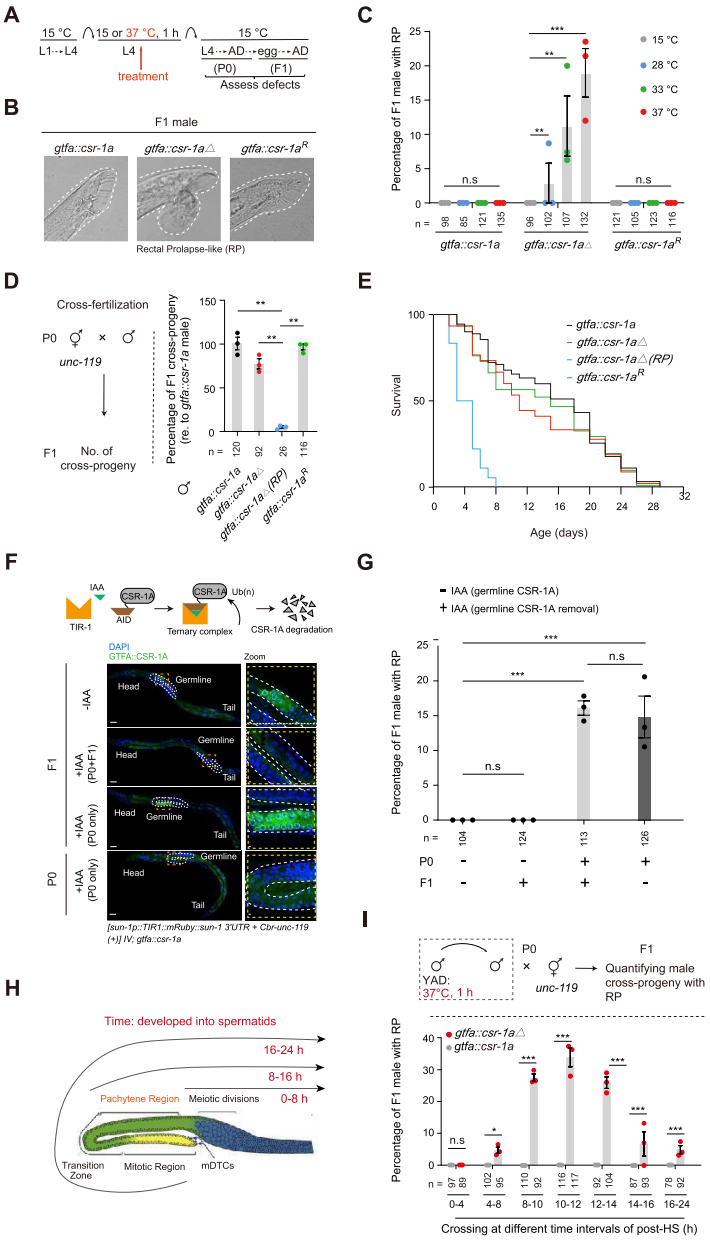

Figure 1. Loss of CSR-1A in the germline causes male offspring with RP, mating interference and being fatal under acute heat stress. (**A**) Schematic of heat stress analysis. P0, parent; F1, the offspring of the first generation; L1 and L4, Larve stage 1 and Larve stage 4; AD, adult worm. (**B**) Representative micrographs showing DIC images of late L4 parental heat-stress-induced F1 male tails in different groups: *gtfa::csr-1a (ezs435)*, *gtfa::csr-1a△ (ezs436)*, and *gtfa::csr-1a^R (ezs437)*. △, *csr-1a* CDS containing the frame-shift mutation. *R*, corrected *csr-1a* reading frame. The protruding dashed lines indicate the tail morphology of F1 males. F1 male tail showed RP-like defect in the *gtfa::csr-1a△ (ezs436)* strain. Scale bar, 5 μm. (**C**) Percentage of F1 male progeny with a RP defect in different groups when late L4 parental hermaphrodites were exposed to different temperatures (15°C, 28°C, 33°C, and 37°C) for 1 h of heat stress. The number of analyzed males in each group is listed. (**D**) Cross ability of F1 male progeny in different groups mated with *unc-119* hermaphrodites when P0 hermaphrodites at late L4 stage were exposed to 37°C for 1 h. The number of cross-progeny males analyzed in each group is listed. For each group, five males were mated with one hermaphrodite. $n = 3$ experiments. (**E**) The survival rate of F1 male progeny in different groups when late L4 parental hermaphrodites were exposed to HS (37°C, 1 h). *gtfa::csr-1a△ (RP)* indicates *gtfa::csr-1a△* male progeny with RP defect. Total number of worms for each group in *gtfa::csr-1a (ezs435)*, *gtfa::csr-1a△ (ezs436)*, and *gtfa::csr-1a^R (ezs437)* is 90. Total number of worms in *gtfa::csr-1a△ (RP)* is 54. (**F**) Representative micrographs showing specific degradation of GFP::TEV::2 × FLAG::AID::CSR-1A expression in pachytene spermatocytes of F1 *gfp::tev::2 × flag::aid::csr-1a; [sun-1p::TIR1::mRuby::sun-1 3′UTR + Cbr-unc-119 (+)] chr IV (ezs462) worms* and P0 worms when fed with IAA. The worms were either fed with (+) or without (-) IAA in P0 and F1 worms or fed with IAA only in P0 worms. Scale bar, 20 μm. The dashed lines indicate the germline of the hermaphrodite worm. The zoomed-in panel on the right shows GFP::TEV::2 × FLAG::AID::CSR-1A expression in pachytene germ cells. Scale bar, 5 μm. (**G**) Percentage of male progeny with a RP defect in worms with (+) or without (-) specific degradation of GFP::TEV::2 × FLAG::AID::CSR-1A in pachytene spermatocytes in P0 or F1 worms upon P0 heat stress at late L4 stage. The number of analyzed males in each group is listed. (**H**) Cartoons depicting the male *C. elegans* germline. Different regions of spermatocytes are shown, with 0–8, 8–16, and 16–24 h representing the time required for the different regions of spermatocytes to mature into round spermatids. (**I**) Percentage of F1 male with a RP defect in *gtfa::csr-1a (ezs435)* and *gtfa::csr-1a△ (ezs436)* groups when P0 young adult males were exposed to 37°C for 1 h of heat stress and crossed with *gtfa::csr-1a; unc-119 (ezs438)* and *gtfa::csr-1a△; unc-119 (ezs439)* hermaphrodites, respectively, at different time intervals (0–4, 4–8, 8–10, 10–12, 12–14, 14–16, 16–24 h) after heat stress (HS). The number of analyzed males in each group is listed. n.s represents no significant difference, $*P < 0.05$; $**P < 0.01$; $***P < 0.001$; $****P < 0.0001$ (*t*-test and one-way ANOVA).

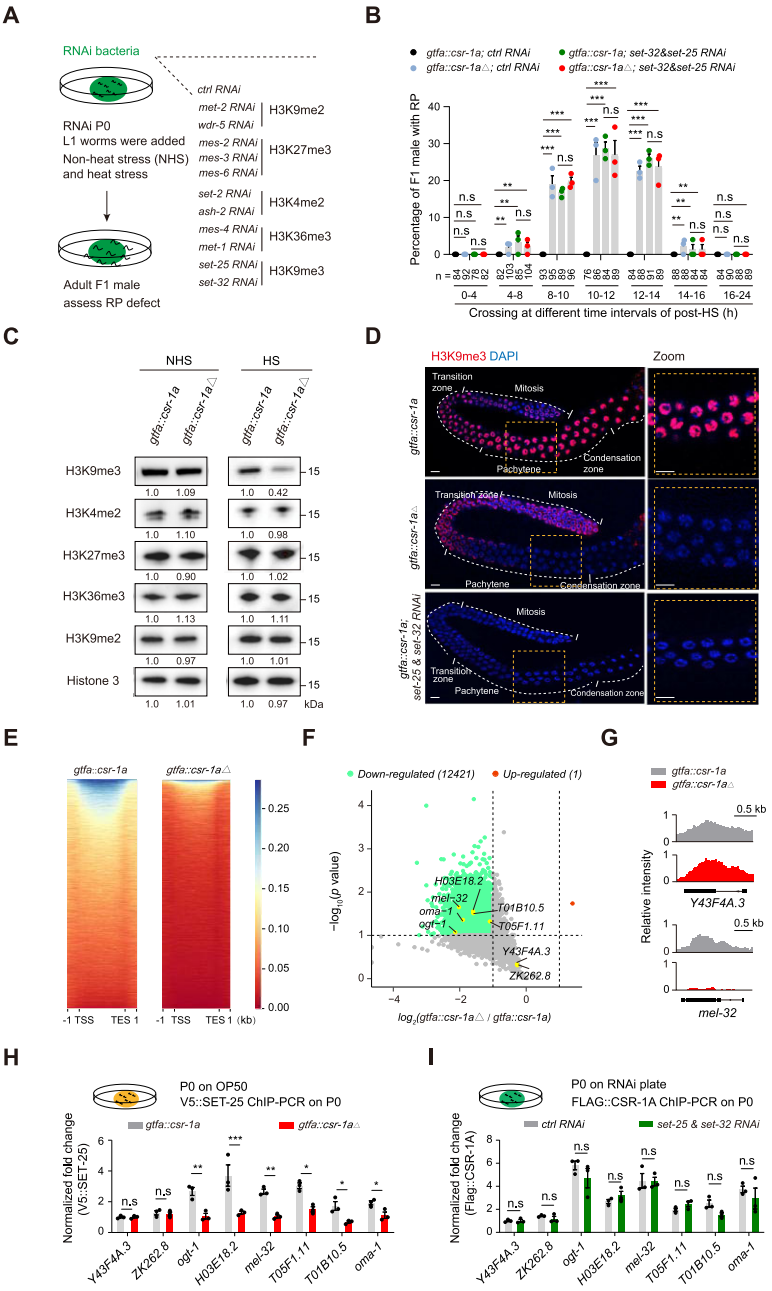

Figure 2. CSR-1A counters heat-stress-induced H3K9me3 reduction in pachytene spermatocytes through SET-25 and SET-32 recruitment. (**A**) This schematic of RNAi screening on genes encoding methyltransferases for analyzing parental heat-stress induced F1 male progeny with RP defects. RNAi bacteria are highlighted in green. (**B**) Percentage of F1 male cross-progeny with RP defect in four groups (gtfa::csr-1a (ezs435); control RNAi, gtfa::csr-1a (ezs435); set-25 & set-32 RNAi, gtfa::csr-1aΔ (ezs436); control RNAi, and gtfa::csr-1aΔ (ezs436); set-25 & set-32 RNAi). Young adult males from the four groups were exposed to HS (37°C, 1 h), respectively. Afterward, they were crossed with hermaphrodites of gtfa::csr-1a; unc-119 (ezs438) or gtfa::csr-1aΔ; unc-119 (ezs439) at different time intervals (0–4, 4–8, 8–10, 10–12, 12–14, 14–16, 16–24 h) following heat-stress. The numbers of males analyzed in each group are provided. (**C**) The western blot image shows the protein levels of H3K9me3, H3K4me2, H3K27me3, H3K36me3, H3K9me2, and Histone 3 in round spermatids isolated from young males of two worm strains: *gtfa::csr-1a; him-8 (ezs441) and gtfa::csr-1aΔ; him-8 (ezs442)*. The samples were collected under two conditions: without heat-stress (NHS) and 8–10 h after heat-stress (37°C, 1 h). (**D**) These micrographs display the immunostaining of H3K9me3 (red) in the male *C. elegans* germline after HS (37°C, 1 h). Scale bar, 10 μm (left), and 3 μm (right). DAPI: blue. (**E**) Heatmaps illustrate the occupancies of H3K9me3 CUT&Tag signals over the gene body in round spermatids isolated from heat-stressed males (*gtfa::csr-1a; him-8* (*ezs441*) and *gtfa::csr-1aΔ; him-8* (*ezs442*)). The samples were collected at 8–10 h post-HS (37°C, 1 h). The other two biological repeats were shown in Supplementary Fig. S2H. (**F**) This plot displays the variations of H3K9me3 CUT&Tag signals in round spermatids isolated from heat-stressed males. The color represents different H3K9me3 CUT&Tag signals compared to *gtfa::csr-1a; him-8* group: upregulated (red), downregulated (green), and unchanged (grey). Genes that were decreased in CUT&Tag analysis were summarized in Supplementary Table S3. FDR = 2, $P = 0.01$. (**G**) The genome browser screenshots demonstrate the H3K9me3 levels at genes of *Y43F4A.3* and *mel-32*, shown in yellow in (**F**). (**H**) The ChIP-PCR graph shows the enrichment of 3 × V5::SET-25 at representative genes, shown in yellow in (**F**), normalized to *Y43F4A.3*. Samples were collected from late L4 worms (*gfp::tev::2 × flag::aid::csr-1a; 3 × V5::set-25* (*ezs443*) *and gfp::tev::2 × flag::aid::csr-1aΔ; 3 × V5::set-25* (*ezs444*)) after heat stress. $n = 3$ experiments. (**I**) The ChIP-PCR graph represents the enrichment of 2 × Flag::CSR-1A at representative genes, shown in yellow in (**F**), normalized to *Y43F4A.3*. Samples were collected from late L4 worms of *gtfa::csr-1a* worms feeding with control RNAi or *set-25* and *set-32* RNAi upon HS. $n = 3$ experiments. n.s means no significant difference, $^{*}P < 0.05$; $^{**}P < 0.01$; $^{***}P < 0.001$; $^{****}P < 0.0001$ (t-test and one-way ANOVA).

Consistent with western blot results, immunofluorescence analyses revealed that H3K9me3—normally abundant throughout the wild-type male germline—was present in the distal region but absent from the pachytene and condensation regions in heat-stressed *csr-1a* mutant germlines (Fig. 2D, Supplementary Fig. S2B, D, and E). By comparison, *set-25/32* RNAi dramatically reduced H3K9me3 staining throughout the male germline.

To determine how the loss of CSR-1A affects H3K9me3 occupancy across the genome in sperm, we used CUT&Tag to profile H3K9me3 occupancy in sperm isolated from heat-stressed *csr-1a*-mutant males or from *wild-type* males (Supplementary Fig. S2F-S2G, Methods). We observed a decrease in the overall H3K9me3 peaks associated with individual genes in *csr-1a (gtfa::csr-1aΔ; him-8 (ezs442)*) mutant sperm compared to *wild-type (gtfa::csr-1a; him-8 (ezs441)*) (Fig. 2E, Supplementary Fig. S2H and O). Indeed, H3K9me3 levels were significantly reduced at most loci in heat-stressed *csr-1a*-mutant sperm (Fig. 2F). H3K9me3 occupancy was reduced across each chromosome, with some exceptional loci (Supplementary Fig. S2I). Representative snapshots of CUT&Tag tracks indicate that if H3K9me3 is reduced in the absence of CSR-1A, it is reduced across the entire locus—from TSS to termination site (Fig. 2G, Supplementary Fig. S2J). Changes in H3K9me3 levels, as revealed by the CUT&Tag assay, were confirmed using H3K9me3 chromatin immunoprecipitation (ChIP) followed by quantitative PCR (Supplementary Fig. S2K). Together our findings suggest that in the absence of CSR-1A, heat stress disrupts H3K9me3 deposition in developing spermatids or that CSR-1A is required to maintain H3K9me3 levels in paternal germ cells after heat stress.

To determine if CSR-1A is required for SET-25 and SET-32 enrichment at loci where CSR-1A is required to maintain H3K9me3 levels after heat stress, we heat-stressed *wild-type* and *csr-1a* mutant worms at late L4 stage and performed SET-25 and SET-32 ChIP assays. In heat-stressed *csr-1a* mutants, SET-25 and SET-32 were reduced at loci where H3K9me3 levels were reduced, but not where H3K9me3 levels remain unchanged (Fig. 2H, Supplementary Fig. S2L–N). By contrast, *set-25/32* RNAi did not significantly affect CSR-1A enrichment at loci with diminished H3K9me3 levels after heat stress (Fig. 2I). Together, these results suggest that CSR-1A promotes the recruitment of SET-25 and SET-32 and H3K9me3 modification in response to heat-stress.

CSR-1A interacts with SET-25/32 through RG motif to prevent RP

CSR-1A could directly or indirectly promote the recruitment of SET-25 and SET-32. Western blot analyses showed that SET-25 and SET-32 levels are similar in *wild-type* and *csr-1a* mutants (Supplementary Fig. S3A and B), indicating that CSR-1A does not regulate the expression of SET-25 or SET-32. To determine if CSR-1A interacts with SET-25 or SET-32, we performed co-immunoprecipitation (co-IP) experiments using strains (*gtfa::csr-1a;3 × v5::set-25 (ezs443), gtfa::csr-1aΔ;3 × v5::set-25 (ezs444), gtfa::csr-1a;set-32::3 × v5 (ezs445) and gtfa::csr-1aΔ;set-32::3 × v5 (ezs446)*) expressing 2 × Flag::CSR-1A, 3 × V5::SET-25, or SET-32::3 × V5 from the endogenous loci. In reciprocal co-IP experiments, we observed heat–stress-dependent co-IP of CSR-1A with SET-25 and SET-32 (Fig. 3A and B, Supplementary Fig. S3C and D). Moreover, co-IP experiments from nuclear and cytoplasmic fractions indicate that CSR-1A and SET-25 or SET-32 primarily interact in the nucleus (Fig. 3B, Supplementary Fig. S3D). Indeed, a small amount of CSR-1A is detected in the nuclear fractions by western blot and in germline nuclei by immunofluorescence (Fig. 3B and C, Supplementary Fig. S3D).

In addition to conserved SET domains that catalyze H3K9 trimethylation [64, 65], most SET-25 homologs possess a highly conserved chromodomain (Supplementary Fig. S3E), which is structurally akin to the Tudor domain and forms an aromatic cage that recognizes lysine and arginine residues [66–68]. The N-terminal disordered region (1–159 aa) of CSR-1A contains 15 RG/RGG motifs (Fig. 3D, top), we therefore wondered if the RG/RGG motif of CSR-1A and the chromodomains of SET-25 or SET-32 are required for their interaction *in vivo*. We used CRISPR to mutate the RG/RGG motif, recoding the first 7 (*csr-1a 7xRG-to-AG*) or all 15 (*csr-1a 15xRG-to-AG*) arginines to alanine or deleting the first exon (*csr-1a* Δexon-1) (i.e. the entire disordered domain or the entire DNA sequence encoding the first exon of CSR-1A) of CSR-1A. Although the structures of *C. elegans* SET-25 and SET-32 have not been determined, we predicted their structures using AlphaFold and identified a putative chromodomain in SET-25 (amino acids 296–386; Fig. 3E). We then used CRISPR to delete the entire *N*-terminal region of SET-25 (up to the SET domain, *set-25 ΔN terminus*), the putative chromodomain only (*set-25 ΔChromodomain*), or the SET domain (*set-25 ΔSET*) (Fig. 3F). Co-IP experiments revealed that recoding all 15 arginines to alanines or deleting the disordered domain prevents CSR-1A from interacting with SET-25 and SET-32 in response to heat stress (Fig. 3D, down and Supplementary Fig. S3F). Moreover, deletions that remove the putative chromodomain of SET-25 prevent it from co-immunoprecipitating with CSR-1A (Fig. 3G).

Lastly, we asked if mutations that disrupt interactions between CSR-1A and SET-25 or SET-32 also disrupt the epigenetic response to heat stress. Compared to *wild-type* worms, the *csr-1a 7xRG-to-AG*, *15xRG-to-AG*, and *Δexon-1* mutants all produced RP male progeny (Fig. 3H). The frequency of RP progeny was higher from the *15xRG-to-AG* and *Δexon-1* mutants than from the *7xRG-to-AG* mutant, consistent with the observation that *7xRG-to-AG* retains some ability to interact with SET-25 and SET-32 (Fig. 3D, Supplementary Fig. S3F). Notably, when combined with *set-32* RNAi, the *set-25* Δchromodomain mutant also produced RP male progeny (Fig. 3H). As expected, neither *set-25* Δchromodomain nor *set-32* RNAi alone produced RP male progeny. These results therefore suggest that, in response to heat stress, CSR-1A employs its RG motif to interact redundantly with the SET-25 chromodomain or SET-32, recruiting the methyltransferases to chromatin targets to maintain or restore their H3K9 trimethylation status and paternal epigenetic programs.

CSR-1A potentiates the recovery of H3K9me3 in germ cells post-heat stress

In response to heat stress, H3K9me3 levels of *C. elegans* germline reportedly decline and gradually recover as cells return to normal [19, 69]. We therefore sought to determine how CSR-1A affects the dynamics of H3K9me3 recovery in pachytene germ cells after heat stress. In order to isolate GFP-positive germ cells by fluorescence-activated cell sorting

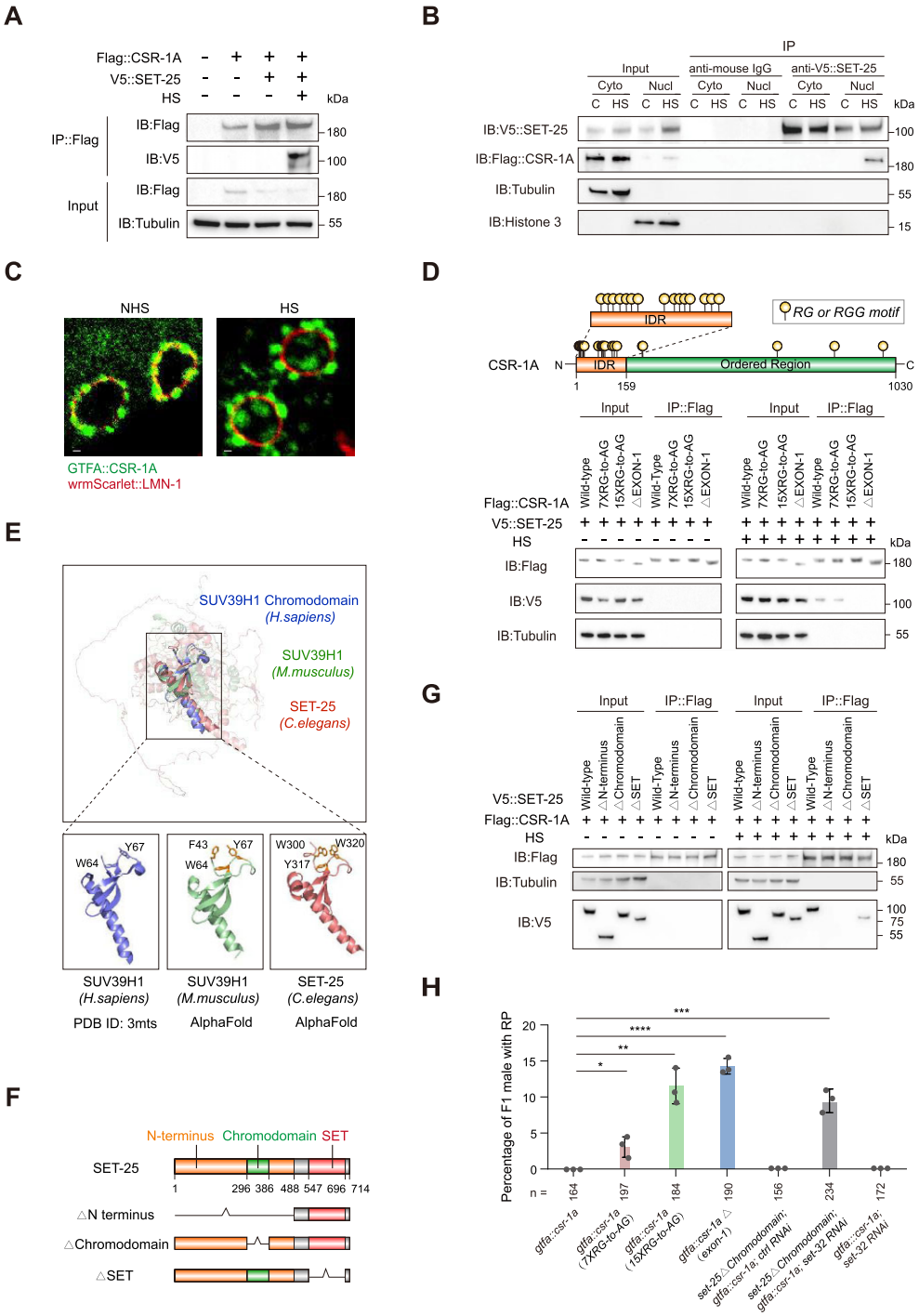

Figure 3. CSR-1A interacts with H3K9me3 methyltransferase SET-25 through RG motif to protect rectal development under heat stress. (**A**) A representative western blot from a co-immunoprecipitation experiment indicates the interaction between 2 × Flag::CSR-1A and 3 × V5::SET-25 upon HS using an anti-Flag antibody. Lysates were collected from late L4 stage worms expressing these proteins and subjected to either HS or no treatment. The experiment included 10% of the input. (**B**) Representative western blot from a co-immunoprecipitation experiment using an anti-V5 antibody. The experiment was performed with nuclear or cytoplasmic extracts from worms expressing 2 × Flag::CSR-1A and/or 3 × V5::SET-25, treated with or without HS. IB, immunoblot. (**C**) Micrographs showing the nucleus of pachytene germ cells in worms with or without heat stress (HS or NHS). Scale bar, 0.5 μm. (**D**) Representative western blot from a co-immunoprecipitation experiment using the Flag antibody to evaluate the interaction between different variants of CSR-1A and SET-25. The experiment was performed with lysates from worms expressing different variants of *flag::csr-1a* and *3 × V5::set-25*, treated with or without HS. The top panel shows a chart of the RG or RGG motif-rich amino-terminal sequence in CSR-1A. (**E**) Superimposed representations of the chromodomain in SUV39H1 (*M.musculus*), SET-25 (*C. elegans*), and SUV39H1 (*H.sapiens*) illustrate their similarity when recognizing and binding with arginine. (**F**) A schematic of the N-terminus, chromodomain, and SET domain of SET-25 and its deletion variants. (**G**) Representative western blot from a co-immunoprecipitation experiment using the flag antibody to evaluate the interaction between different variants of SET-25 and CSR-1A. The experiment was performed with lysates from worms expressing different variants of *3 × V5::set-25* and *flag::csr-1a*. (**H**) Percentage of male progeny with RP defect in different groups of worms when exposed to HS. The worms used in the experiment include different variants of CSR-1A or SET-25 proteins. The numbers of analyzed males in each group are listed. n.s indicates no significant difference, $*P < 0.05$; $**P < 0.01$; $***P < 0.001$; $****P < 0.0001$ (one-way ANOVA).

(FACS), we created *wild-type* and *csr-1a*-mutant worms that only express GFP in germ cells of L4 hermaphrodites. We inserted in-frame *gfp::tev::2xflag::aid* coding sequences immediately after the start codon of *wild-type csr-1a*, generating *gfp::tev::2xflag::aid::csr-1a* (*ezs435*) worms. Because the *csr-1aΔ* frameshift would destabilize a *gfp::tev::2xflag::aid::csr-1aΔ* fusion transcript, we inserted an intercistronic region with an SL2 trans-spliced leader sequence between the GFP and 2 × Flag coding sequences (*gfp::sl2::2xflag::aid::csr-1aΔ (ezs458)*), thereby uncoupling the stability of the *gfp* mRNA from that of the *2xflag::aid::csr-1aΔ* mRNA (Supplementary Fig. S4A and B). We then disrupted 10 million late-L4-staged worms from each strain, isolated GFP-positive germ cells by FACS, and measured H3K9me3 levels by western blot at various times after heat stress (Fig. 4A, Supplementary Fig. S4C–E). H3K9me3 levels were reduced by ∼75% in both wild-type and *csr-1a*-mutant GFP-positive germ cells immediately ($t = 0$) after heat stress, but whereas H3K9me3 levels were fully recovered within 20 min in *gfp::tev::2xflag::aid::csr-1a* GFP-positive germ cells, recovery was slower and incomplete in *gfp::sl2::2xflag::aid::csr-1a* GFP-positive germ cells (Fig. 4B and C). Thus, CSR-1A appears to facilitate the swift recovery of H3K9me3 levels.

Our CUT&Tag analyses show that CSR-1A loss of function reduces H3K9 trimethylation at >12 000 genes (Fig. 2F), but previous studies showed that CSR-1A recognizes >2000 genes via its 22G-RNA guide sequences [38, 39]. These results suggest that CSR-1 promotes the recovery of H3K9me3 levels on many genes that are not CSR-1A 22G-RNA targets. To gain insight into how CSR-1A regulates H3K9 trimethylation of its targets (group A genes) and non-targets (group B genes), we used H3K9me3 ChIP to analyze several group A genes (*oma-1, B0252.5, and F13H10.3)* and group B genes (*F13H8.2, unc-38, and attf-2*), as well as a set of "control" genes (e.g. *K08D12.6*, *abu-8* and *nhr-15*) with low H3K9me3 levels that do not respond to heat stress or CSR-1A activity. We heat-stressed *wild-type*, *csr-1aΔ*, and *15xRG-to-AG* GFP-positive germ cells and measured H3K9me3 levels at $t = 0$, 10, and 30 min after heat shock. As expected, H3K9me3 levels were lower on control genes than on groups A and B and were unaffected by heat stress or *csr-1a* genotype (Fig. 4D-i and iv). By contrast, heat stress rapidly depleted H3K9me3 levels on group A and group B genes. Their levels rapidly recovered in the presence of wild-type CSR-1A but remained strongly depleted in *csr-1a* mutant cells (Fig. 4D-ii–vi). Notably, in wild-type cells, H3K9me3 levels on group A genes recovered faster than on group B genes (Fig. 4D-iv). Additionally, we observed that group B genes (i.e. non-targets) are of 2000–2500 base pair (bp) relative distance to the transcription start site (TSS) of group A genes (i.e. CSR-1A targets; Fig. 4D top). These results suggest that, following heat stress in male germ cells, CSR-1A potentiates the rapid restoration of H3K9me3 on CSR-1A target genes. 22G-RNAs guide their associated CSR-1A to recognize and bind to >2000 genes [38, 39]. To see whether CSR-1A promoting the rapid restoration of H3K9me3 on its target genes is small RNA-dependent or not, we found that following parental heat stress, mutation of RNA-dependent RNA polymerase (RdRP) genes, *ego-1* and *rrf-3*, which are involved in the 22G-RNAs amplification pathway [33, 38, 70], induced male progeny with RP defects (Supplementary Fig. S4F), suggesting that CSR-1A promoting the rapid restoration of H3K9me3 on CSR-1A target genes is small RNA-dependent.

Developmental defect of rectal valve and gland cells relates to RP

In addition to its expression in pachytene germ cells (Supplementary Fig. S5A) [38, 39], CSR-1A protein is highly expressed in tail cells throughout post-embryonic development (Fig. 5A and B, Supplementary Fig. S5A). Cell-specific markers revealed that GFP::CSR-1A is expressed in two rectal valve cells (labeled with wrmScarlet::PCS-1) [71] and three rectal gland cells (labeled with wrmScarlet::PNC-1) [72] (Fig. 5C). These tail cells—referred to herein as RVRG cells—gradually grow in size during normal male development (Fig. 5D). In male progeny of heat-stressed *csr-1a* fathers, however, RVRG cells gradually diminished in size during the L4 stage and were absent in RP males (Fig. 5E–G, Supplementary Fig. S5D–F). Thus CSR-1A appears to enforce a heat-sensitive epigenetic program required for the growth and survival of RVRG cells. Because our genetic tests suggested that paternal germline CSR-1A enforces this program (Fig. 1F and G, Supplementary Fig. S1G and H). This prompted us to investigate whether CSR-1A in the parental germline or RVRG cells plays a more significant role in preventing RP defects in male offspring. We used the auxin-responsive degron system to deplete CSR-1A only in RVRG cells (Supplementary Fig. S5B). Compared to ∼15% of the male offspring developing the RP phenotype when parental germline CSR-1A was depleted (Fig. 1F and G), we observed that ∼3% of the male offspring developed the RP phenotype when depleting CSR-1A only in RVRG cells (Supplementary Fig. S5C), suggesting that CSR-1A in the paternal germ cells mainly ensures the normal development of RVRG of male offspring under heat stress.

CSR-1A loss upregulates the cytoskeleton-related genes in RVRG cells

To investigate how parental CSR-1A promotes the growth and survival of offspring RVRG cells following paternal heat stress, we analyzed the expression profiles of RVRG cells isolated from the offspring of heat-stressed *wild-type* or *csr-1a*-mutant parents (Fig. 6A, Supplementary Fig. S6A and B). We disrupted *wild-type* (*gfp::sl2::2xflag::aid::csr-1a*) and *csr-1a* mutant (*gfp::sl2::2xflag::aid::csr-1aΔ*) worms expressing RVRG markers (*pnc-1p::wrmScarlet* and *pcs-1p::wrmScarlet*) and to isolated the GFP + wrmScarlet + RVRG cells by FACS. *Wild-type (N2)* worms without fluorescent reporters served as negative controls for cell sorting. To increase the population of males, we introduced a *him-8* mutation into each strain. We then used RNA sequencing (RNA-seq) to analyze the gene expression profiles in RVRG cells. Principal component analysis (PCA) of the RNA-seq data showed that paternal heat stress induces clear gene expression differences between *wild-type* and *csr-1a*-mutant RVRG cells (Supplementary Fig. S6C), with 363 genes upregulated and 61 genes downregulated in *csr-1a*-mutant worms compared to wild type (Fig. 6B). Gene Ontology (GO) analysis of the upregulated genes revealed an enrichment of genes associated with muscle differentiation and development, cytoskeleton organization, and morphology/morphogenesis (Fig. 6C).

To assess the effect of CSR-1A on a role in the cytoskeletal organization of RVRG cells (Fig. 6C), we examined a fusion between actin and wrmScarlet (Lifeact::wrmScarlet) [73]. We observed more actin aggregates in the male progeny from heat-stressed *csr-1a* mutant males than from wild-type worms (Fig. 6D). Actin aggregation can lead to cell death

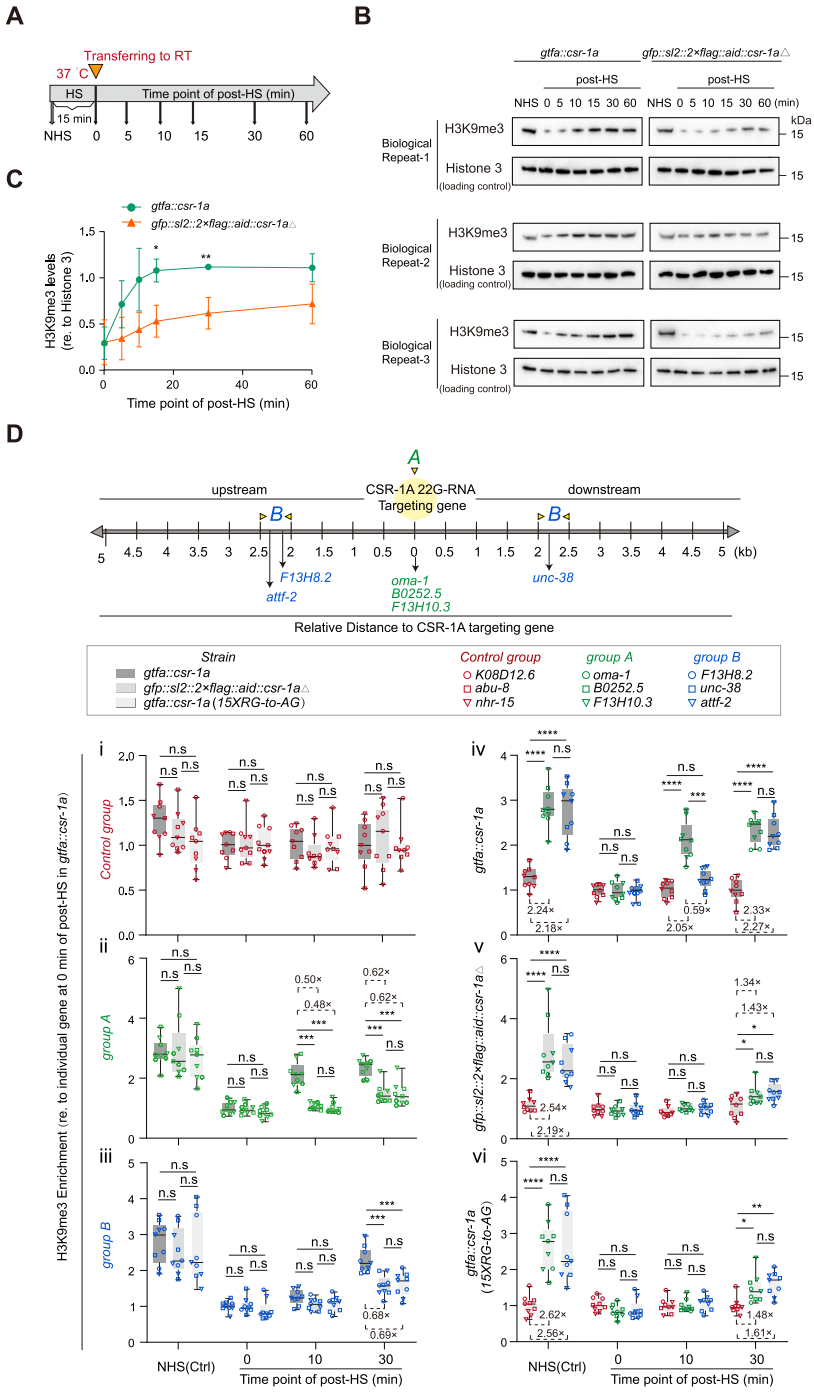

Figure 4. CSR-1A potentiates the recovery of H3K9me3 from heat-stress-induced decline, likely through initiating from CSR-1A-targeted genes. (**A**) Schematic diagram showing an overview of the experimental setup. It shows the exposure of CSR-1A-expressing germ cells to heat stress (37°C, 15 min) and the subsequent recovery timeline. Temperatures in this experiment are highlighted in red. (**B**) Western blot analysis was performed on germ cells isolated from late L4 stage worms (*gtfa::csr-1a* (*ezs435*) and *gfp::sl2::2* × *flag::aid::csr-1a*△ (*ezs458*)) with or without heat stress, at various time points (0, 5, 10, 15, 30, and 60 min) during the recovery phase. Three biological repeats were performed. (**C**) Higher H3K9me3 recovery rate after HS in *gtfa::csr-1a (ezs435)* group. The data from (**B**) is quantified and normalized to the levels of Histone 3 (loading control). Quantified replicate data of H3K9me3 fluorescence intensity (normalized to Histone 3) are shown in Supplementary Table S5. (**D**) ChIP-PCR analysis shows the enrichment of H3K9me3 in germ cells expressing different forms of CSR-1A under various conditions during recovery (0, 10, and 30 min) post HS. The germ cells were isolated from late L4 worms of *gtfa::csr-1a (ezs435), gtfa::csr-1a (15 × RG to AG) (ezs449), and gfp::sl2::2 × flag::aid::csr-1a*△ *(ezs458)* expressing wild-type CSR-1A, CSR-1A with an RG-to-AG mutation, or no CSR-1A, with or without heat stress. The enrichment was normalized to individual gene at 0 min of post heat-stress in *gtfa::csr-1a* group. The top panel shows a cartoon illustrating the relative distance of promoters (TSS) of genes that were downregulated in CUT-Tag analysis (*gtfa::csr-1a*△*; him-8* (*ezs442*) versus *gtfa::csr-1a; him-8* (*ezs441*)) to the nearest promoters of CSR-1A 22G-RNA targeting genes. The genes were categorized into *group A* (genes downregulated in CUT-Tag analysis and CSR-1A 22G-RNA targeting genes, highlighted in green), *group B* (genes downregulated in CUT-Tag analysis within a specific relative distance to CSR-1A 22G-RNA targeting genes, highlighted in blue), and *Control group* (genes neither downregulated in CUT-Tag analysis nor CSR-1A 22G-RNA targeting genes, highlighted in red). Three representative genes were randomly chosen for each group. $n = 3$ experiments. n.s means no significant difference, $*P < 0.05$; $**P < 0.01$; $***P < 0.001$; $****P < 0.0001$ (one-way ANOVA).

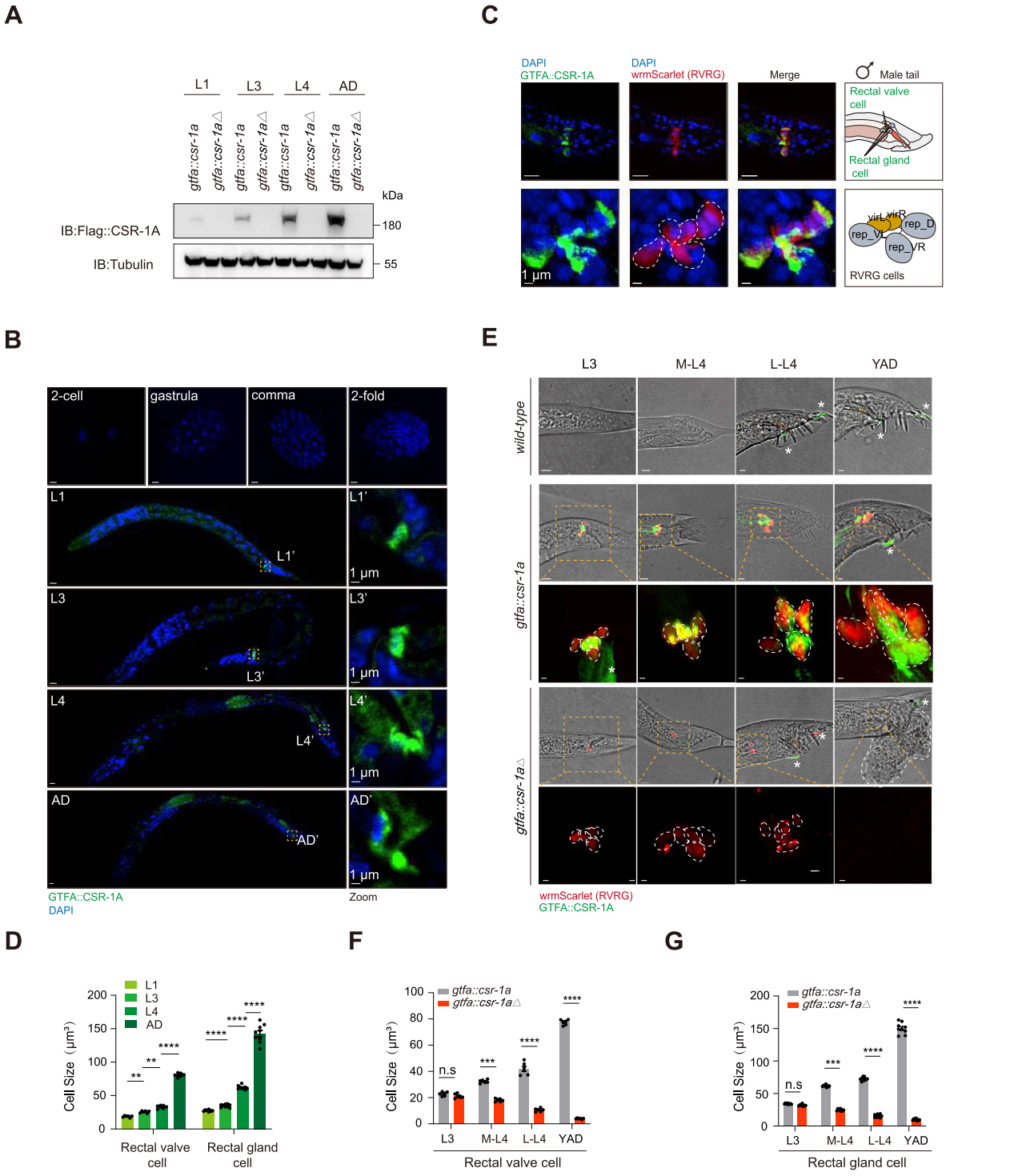

Figure 5. Collapse of developmental rectal valve and gland cells correlates with RP post-heat stress. (**A**) A representative western blot shows the expression of 2 × Flag::CSR-1A in *gtfa::csr-1a* and *gtfa::csr-1a*△ worms at different stages of development. Antibodies against flag and tubulin were used. (**B**) Representative micrographs displaying the expression of CSR-1A in RVRG cells during different developmental stages of *C. elegans*, from the embryonic stage to adulthood. The right panel zooms in on the CSR-1A expression in RVRG cells. Scale bar, 5 μm (left). (**C**) Representative micrographs demonstrate the co-localization of CSR-1A (GFP) and PCS-1/PNC-1 (wrmScarlet) in the rectal valve and gland (RVRG) cells of the male *C. elegans* tail. The bottom panel shows the projections of confocal z sections through RVRG cells, with dashed lines indicating the vir and rep (RVRG) cells. A model illustrating the structure of RVRG cells in the male tail is also shown. Scale bar, 3 μm. (**D**) Quantification of the size of male RVRG cells at different developmental stages, as measured in 6–9 experiments. (**E**) Representative micrographs using specific markers showing the morphological changes in RVRG cells during the formation of the male tail (L3 to young adult), along with RP defects, in different groups of worms, including N2 (*wild-type*) group, *gtfa::csr-1a; Ex (pnc-1p::wrmScarlet); Ex (pcs-1p::wrmScarlet) (ezs460) and gtfa::csr-1a*△*; Ex (pnc-1p::wrmScarlet); Ex (pcs-1p::wrmScarlet) (ezs461) group* with parental L4 heat-stress. Scale bar, 5 μm. A zoomed-in 3D image of RVRG cells is also shown, with a scale bar of 1 μm. (F and G) Quantification of the size of male rectal valve cells (**F**) and rectal gland cells (**G**) in (**E**) from the L3 to the young adult stage, along with male tail formation, in different groups of worms. The data were obtained from 6 to 9 experiments. n.s represents no significant difference, $*P < 0.05$; $**P < 0.01$; $***P < 0.001$; $****P < 0.0001$ (one-way ANOVA and t-test).

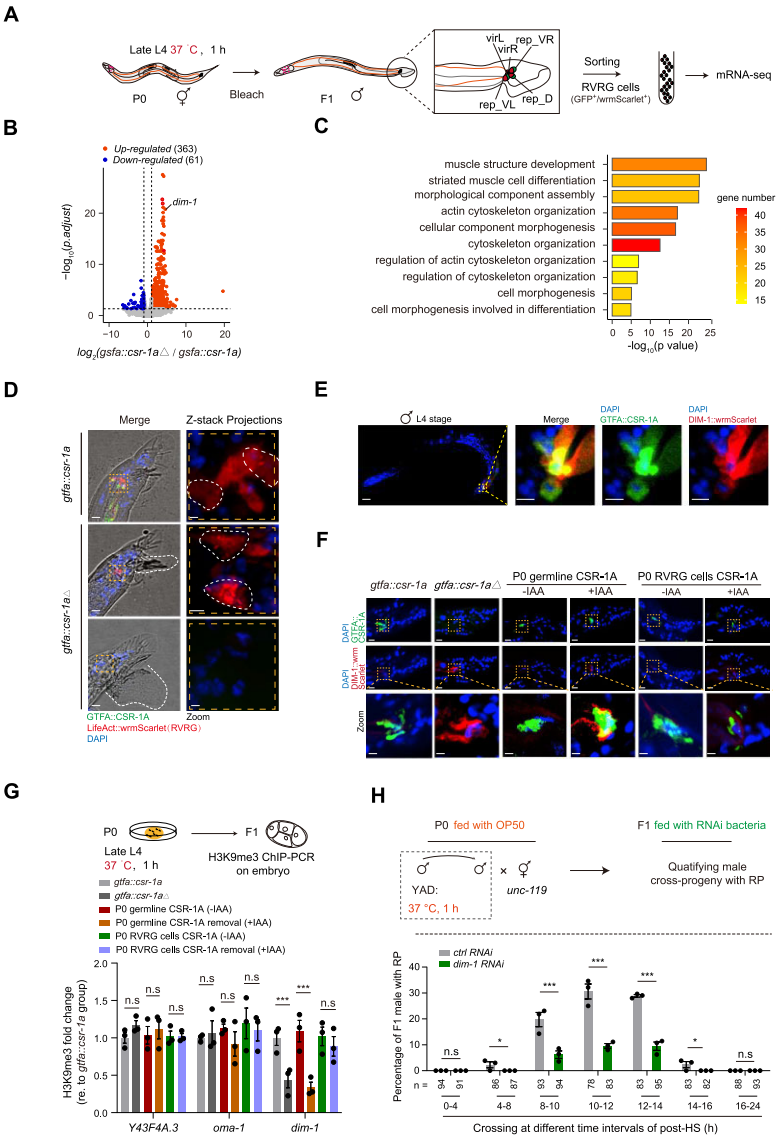

Figure 6. RNA-seq of RVRG cells identified *dim-1* as a key regulator to modulate RP. (**A**) The model illustrates the isolation of RVRG cells from F1 male worms of gfp::sl2::2 × flag::aid::csr-1a; him-9; Ex (pnc-1p::wrmScarlet); Ex (pcs-1p::wrmScarlet) (ezs472) and gfp::sl2::2 × flag::aid:: csr-1aΔ; him-9; Ex (pnc-1p::wrmScarlet); Ex (pcs-1p::wrmScarlet) (ezs473), the late L4 parental worms were subjected to heat stress. Temperatures in this experiment are highlighted in red. (**B**) The plot shows mRNA expression profiling datasets of RVRG cells from the two strains mentioned in (**A**). The fold changes of mRNA expression display *gfp::sl2:: 2 × flag::aid::csr-1aΔ; him-9; Ex (pnc-1p::wrmScarlet);Ex (pcs-1p::wrmScarlet)* (*ezs473, i.e. gsfa::csr-1aΔ)* versus *gfp::sl2::2 × flag::aid::csr-1a; him-8; Ex (pnc-1p::wrmScarlet);Ex (pcs-1p::wrmScarlet)* (*ezs472, i.e. gsfa::csr-1a)*. The color signifies different gene changes, including upregulated genes (red), downregulated genes (blue), and unchanged genes (grey). Upregulated genes are listed in Supplementary Table S4. FDR = 2, $P = 0.05$. (**C**) The GO terms for the upregulated differentially expressed genes in (**B**). (**D**) Representative micrographs depict the actin cytoskeleton (red) in RVRG cells of male progeny tail from two different strains of worms (*gtfa::csr-1a; Ex (pnc-1p::lifeact::wrmScarlet); Ex (pcs-1p::lifeact::wrmScarlet) (ezs470))* and *gtfa::csr-1aΔ;Ex (pnc-1p::lifeact::wrmScarlet);Ex (pcs-1p::lifeact::wrmScarlet)* (*ezs471))* with RP defects after late L4 parental heat stress. Scale bar, 5 μm. Zoomed-in images of LifeAct::wrmScarlet expression in RVRG cells are also shown. Scale bar, 1 μm. GTFA::CSR-1A: green. LifeAct::wrmScarlet: red. DAPI: blue. (**E**) Representative micrographs demonstrate the co-localization of GFP::CSR-1A and DIM-1::wrmScarlet in L4 male *C. elegans* RVRG cells. Scale bar, 10 μm. Zoomed-in images of RVRG cells are also shown. Scale bar, 1 μm. GTFA::CSR-1A: green. DIM-1::wrmScarlet: red. DAPI: blue. (**F**) Representative micrographs of DIM-1::wrmScarlet expression in F1 L4 male *C. elegans* RVRG cells from different experimental groups, including GFP::CSR-1A (*gtfa::csr-1a;dim-1::wrmScarlet (ezs467))*, GFP::CSR-1AΔ *(gtfa::csr-1aΔ;dim-1::wrmScarlet (ezs474))*, and IAA-mediated CSR-1A degradation in either the parental germline (*gtfa::csr-1a;dim-1::wrmScarlet;[Psun-1::tir-1::mRuby::eft 3′ utr] chr IV (ezs468))* or parental RVRG cells (*gtfa::csr-1a;dim-1::wrmScarlet;Ex[Ppnc-1::tir-1::wrmScarlet]; Ex[Ppcs-1::tir-1::wrmScarlet] (ezs469))* after subjecting the parental worms to heat stress at late L4 stage. Scale bar, 4 μm. Zoomed-in images of DIM-1::wrmScarlet and GFP::CSR-1A expression in RVRG cells are also shown. Scale bar, 1 μm. GTFA::CSR-1A: green. DIM-1::wrmScarlet: red. DAPI: blue. **(G)** ChIP-PCR results display the enrichment of H3K9me3 (relative to the wild-type group) in F1 embryos from different experimental groups, including GFP::CSR-1A, GFP::CSR-1AΔ, parental germline CSR-1A degradation, and parental RVRG cells CSR-1A degradation groups, after late L4 parental heat stress. $n = 3$ experiments. Temperatures in this experiment are highlighted in red. (**H**) The percentage of male cross-progeny with RP defects in F1 *gtfa::csr-1aΔ (ezs436)* worms fed with *control* RNAi (highlighted in red) or *dim-1* RNAi (highlighted in green). The parental young adult males were exposed to 37°C heat stress for 1 h (highlighted in red) and at different time intervals after heat stress, were crossed with *gtfa::csr-1aΔ; unc-119 (ezs439)* hermaphrodites. The top panel provides a schematic representation of the experimental setup, and the numbers of analyzed males in each group are listed. n.s indicates no significant difference, $*P < 0.05$; $**P < 0.01$; $***P < 0.001$; $****P < 0.0001$ (one-way ANOVA and *t*-test).

(Supplementary Fig. S7A) [74–76], perhaps consistent with the eventual loss of RVRG cells in RP males.

Muscle cytoskeleton gene *dim-1* RNAi represses RP

The *dim-1* (disorganized muscle-1, a homolog of Titin in *H. sapiens*) gene encodes an immunoglobulin-like protein required for muscle structure and integrity [77]. To visualize the DIM-1 protein, we used CRISPR/Cas9 genome editing to insert an in-frame *wrmScarlet* coding sequence immediately before the endogenous stop codon of *dim-1*. DIM-1::wrmScarlet fluorescence was clearly observed in RVRG cells in *wild-type* worms beginning at the L4 stage of development (Fig. 6E and Supplementary Fig. S7B), but was not detected at earlier developmental stages. Importantly, DIM-1::wrmScarlett was markedly upregulated in RVRG cells in the progeny of either heat-stressed *csr-1a*-mutant or germline *csr-1a*–depletion worms (Fig. 6F, Supplementary Fig. S6D). By contrast, CSR-1A depletion in RVRG cells of heat-stressed parents did not increase DIM-1::wrmScarlet expression in the progeny RVRG cells (Fig. 6F, Supplementary Fig. S6D). We next hypothesized whether the upregulated expression of *dim-1* in RVRG cells is correlated with the decreased H3K9me3 level when CSR-1A is absent in the paternal germline. Consistent with this hypothesis, H3K9 trimethylation of *dim-1* in embryos is reduced if the paternal germ line lacks CSR-1A activity (Fig. 6G). This suggests that H3K9 trimethylation status of *dim-1* in the paternal germ line is heritable and determines its expression level in RVRG cells of male offspring.

To determine if the up-regulation of DIM-1 contributes to the RP phenotype observed in *csr-1a* mutants, we collected *csr-1a* offspring from a heat-stressed paternal cross and used RNAi to silence *dim-1* expression (Fig. 6H, top). Notably, the reduction of DIM-1 partially rescued the RP defect of *csr-1a* mutants (Fig. 6H, down), suggesting that DIM-1 overproduction does indeed contribute to the RP-like phenotype associated with heat stress in the absence of paternal CSR-1A function.

Discussion

Here we have shown that CSR-1A acts in the paternal germline to enforce a heritable epigenetic program required for male tail development. Our results suggest that CSR-1A interacts via its RG motifs with SET-25 and SET-32 histone H3K9 methyltransferases to rapidly restore heat-labile H3K9me3 modifications in male germ cells. This CSR-1A-dependent response to heat stress in the paternal germline maintains the fate of rectal cells in male offspring by suppressing the expression of developmental genes including *dim-1* (Fig. 7).

In previous studies, Argonaute proteins have been shown to defend against viral infections [25–28], resist starvation stress [29, 30], direct behavioral avoidance of pathogens [78], and inhibit transformations induced by plasmids [79, 80]. Our data augments the array of Argonaute functions, demonstrating their role in safeguarding the normal somatic RVRG development of offspring following paternal exposure to environmental heat stress. In addition, extensive evidence suggests that epigenetic information in mouse sperm can be passed on, bypassing post-fertilization reprogramming, and triggering changes in gene expression during embryogenesis [81], thereby influencing pre- and post-implantation embryo development [12, 82, 83–85]. Our findings suggest that epigenetic defects inherited from sperm at developmental regulatory regions can persist throughout embryogenesis and become activated during the late stage of larval development. Given the involvement of H3K9me3 heterochromatin in gene regulation, genome integrity and chromosome organization [68, 86–88], the CSR-1A-dependent repressive H3K9me3 marks in response to heat stress might serve additional functions beyond establishing paternally inherited developmental programs. This possibility merits further investigation.

Increasing studies have demonstrated that both imprinted paternal genes and paternal environmental stress can influence the health of the next generation, with the epigenome potentially playing a crucial role in this process [89–92]. The epigenome can possibly affect the phenotype of subsequent generations through transmission via sperm [12, 82–84]. Notably, spermatogenesis necessitates epigenomic reprogramming and a histone-to-protamine transition, thereby erasing previous epigenetic memories [93]. Interestingly, even after protamines replace histones, about 1% of histone proteins still remain in mature mouse sperm, and up to approximately 15% in human sperm [94–97]. While some histones are removed immediately after fertilization [98], others may persist and influence embryo development [12, 82, 83–85]. These seminal findings suggest that sperm histones marker genes may have a function beyond gene regulation during spermatogenesis, acting as transmitters of paternal epigenetic information [82]. In the study described here, the decline in H3K9me3 at genes following initial stress exposure transmitted memories of prior paternal stress exposure in the absence of CSR-1A. Without paternal stress exposure, such as in routine 20°C cultivation of nematodes, *csr-1a* mutants exhibited no significant abnormal phenotype compared to wild-type animals [38, 39]. However, with paternal stress exposure, CSR-1A likely serves as a rectifier of environmentally altered epigenetic information. It safeguards the developmental program inherited from the father, thereby facilitating the normal somatic development of progeny.

A handful of studies to date have shown that improper alterations in histone methylation may impact paternal imprinted genes, leading to sex-specific consequences [99]. Intriguingly, such epigenetic changes often occur quickly and frequently throughout an organism's reproductive lifespan, but they tend to be lost across just a few generations [100, 101]. In our study, we observed the effect of the disorganized muscle gene *dim-1*, modified by H3K9me3 in the paternal germline, on the later development of male somatic RVRG in the next generation. This finding suggests that paternal epigenetic memory programs the later developmental phenotype of offspring, which may serve to enhance adaptation to environmental changes and uphold population productivity and stability.

Despite our concerted efforts to isolate germ cells from a large cohort of synchronized L4 stage *C. elegans* and examine variations in the total level of H3K9me3 in these germ cells during immediate recovery after heat stress, the lack of a cell culture system for cultivating germ cells limited our further investigation. We did not investigate the genome-wide dynamic chromatin binding footprints of CSR-1A or SET-25/32 following heat stress. Such studies will be important to comprehend the dynamics of CSR-1A or SET-25/32 bind-

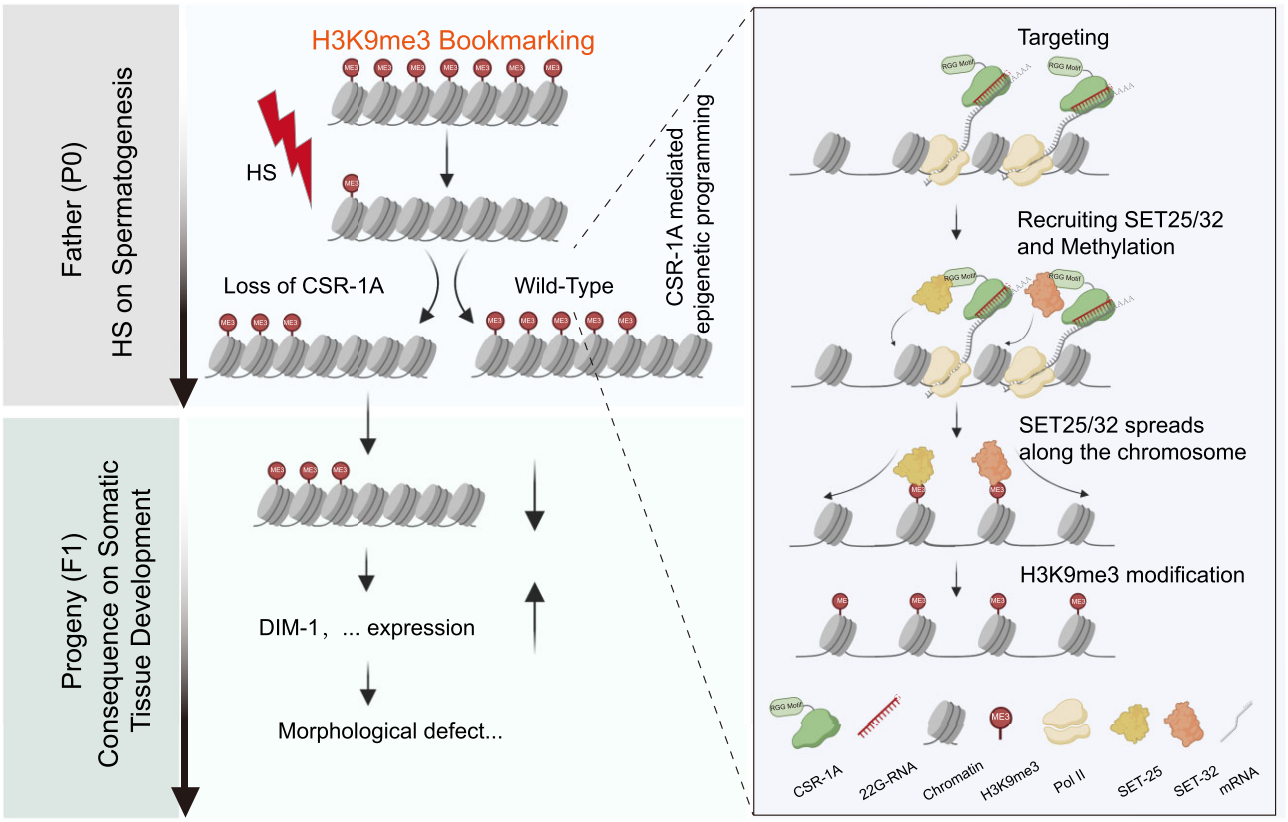

Figure 7. A proposed model illustrating how CSR-1A potentiates the recovery of H3K9me3 in germ cells post-heat stress and its implication in somatic development of next generation.

ing and H3K9me3 modification during recovery from heat stress.

Acknowledgements

We thank C. C. Mello from UMass Chan Medical School and Chun-Qing Song from Westlake University for insightful suggestions; Hongyun Tang laboratory and Dr. Shi Jing for their assistance in cell sorting; Xuejia Li, Zhiqing Li, and Xuanxuan Guo in Shen laboratory and Xiong Xiong in Yanxiao Zhang laboratory for their help in strain construction during revision and discussions. E.-Z.S. acknowledges support from the Westlake Center for Genome Editing, program No.21200000A992210/004, Westlake Education Foundation, Zhejiang Provincial Foundation of China (2021R01013), Westlake Education Foundation (041010140118), the National Natural Science Foundation of China (NSFC32070628), Zhejiang Provincial Key Laboratory Construction Project, and the Westlake Laboratory of Life Sciences.

Author contributions: E.-Z.S. conceptualized the study. D.R., D.-F.L., L.-L.L., J.-C.X., S.-K.T., and E.-Z.S. performed the investigations. E.-Z.S. and D.R. wrote the original draft. E.-Z.S. reviewed and edited the manuscript. E.-Z.S. coordinated the project.

Supplementary data

Supplementary data is available at NAR online.

Conflict of interest

None declared.

Funding

Westlake Center for Genome Editing (Grant/Award Number: '21200000A992210/004'), Westlake Education Foundation, Zhejiang Provincial Foundation of China (Grant/Award Number: '2021R01013'), Westlake Education Foundation (Grant/Award Number: '041010140118'), the National Natural Science Foundation of China (Grant/Award Number: 'NSFC32070628'), Zhejiang Provincial Key Laboratory Construction Project, and the Westlake Laboratory of Life Sciences. Funding to pay the Open Access publication charges for this article was provided by Westlake Education Foundation.

Data availability

CUT-TAG seq data and mRNA seq data are available in the NCBI GEO database: (accession number GSE262243 and GSE262244)

References

1. Dong WY, Zhu X, Tang HD *et al.* Brain regulation of gastric dysfunction induced by stress. *Nat Metab* 2023;5:1494–505. https://doi.org/10.1038/s42255-023-00866-z

2. Kivimaki M, Steptoe A. Effects of stress on the development and progression of cardiovascular disease. *Nat Rev Cardiol* 2018;**15**:215–29. https://doi.org/10.1038/nrcardio.2017.189
3. Lupien SJ, McEwen BS, Gunnar MR *et al.* Effects of stress throughout the lifespan on the brain, behaviour and cognition. *Nat Rev Neurosci* 2009;**10**:434–45. https://doi.org/10.1038/nrn2639
4. Johnstone SE, Baylin SB. Stress and the epigenetic landscape: A link to the pathobiology of human diseases? *Nat Rev Genet* 2010;**11**:806–12. https://doi.org/10.1038/nrg2881
5. Xu X, Miao Z, Sun M *et al.* Epigenetic mechanisms of paternal stress in offspring development and diseases. *Int J Genomics* 2021;**2021**:6632719. https://doi.org/10.1155/2021/6632719
6. Donkin I, Barres R. Sperm epigenetics and influence of environmental factors. *Mol Metab* 2018;**14**:1–11. https://doi.org/10.1016/j.molmet.2018.02.006
7. Wei Y, Schatten H, Sun QY. Environmental epigenetic inheritance through gametes and implications for human reproduction. *Hum Reprod Update* 2015;**21**:194–208. https://doi.org/10.1093/humupd/dmu061
8. Hansen KH, Bracken AP, Pasini D *et al.* A model for transmission of the H3K27me3 epigenetic mark. *Nat Cell Biol* 2008;**10**:1291–300. https://doi.org/10.1038/ncb1787
9. Iwasaki M. Chromatin resetting mechanisms preventing transgenerational inheritance of epigenetic states. *Front Plant Sci* 2015;**6**:380. https://doi.org/10.3389/fpls.2015.00380
10. Katz DJ, Edwards TM, Reinke V *et al.* A C. elegans LSD1 demethylase contributes to germline immortality by reprogramming epigenetic memory. *Cell* 2009;**137**:308–20. https://doi.org/10.1016/j.cell.2009.02.015
11. Kim DH, Doyle MR, Sung S *et al.* Vernalization: winter and the timing of flowering in plants. *Annu Rev Cell Dev Biol* 2009;**25**:277–99. https://doi.org/10.1146/annurev.cellbio.042308.113411
12. Lismer A, Dumeaux V, Lafleur C *et al.* Histone H3 lysine 4 trimethylation in sperm is transmitted to the embryo and associated with diet-induced phenotypes in the offspring. *Dev Cell* 2021;**56**:671–86. https://doi.org/10.1016/j.devcel.2021.01.014
13. Moazed D. Mechanisms for the inheritance of chromatin states. *Cell* 2011;**146**:510–8. https://doi.org/10.1016/j.cell.2011.07.013
14. Wang F, Higgins JM. Histone modifications and mitosis: countermarks, landmarks, and bookmarks. *Trends Cell Biol* 2013;**23**:175–84. https://doi.org/10.1016/j.tcb.2012.11.005
15. Xing H, Vanderford NL, Sarge KD. The TBP-PP2A mitotic complex bookmarks genes by preventing condensin action. *Nat Cell Biol* 2008;**10**:1318–23. https://doi.org/10.1038/ncb1790
16. Zhang Y, Zhang X, Shi J *et al.* Dnmt2 mediates intergenerational transmission of paternally acquired metabolic disorders through sperm small non-coding RNAs. *Nat Cell Biol* 2018;**20**:535–40. https://doi.org/10.1038/s41556-018-0087-2
17. Feng X, Li C, Zhang H *et al.* Heat-stress impacts on developing bovine oocytes: unraveling epigenetic changes, oxidative stress, and developmental resilience. *Int J Mol Sci* 2024;**25**:4808. https://doi.org/10.3390/ijms25094808
18. Das S, Min S, Prahlad V. Gene bookmarking by the heat shock transcription factor programs the insulin-like signaling pathway. *Mol Cell* 2021;**81**:4843–60. https://doi.org/10.1016/j.molcel.2021.09.022
19. Klosin A, Casas E, Hidalgo-Carcedo C *et al.* Transgenerational transmission of environmental information in *C. elegans*. *Science* 2017;**356**:320–3. https://doi.org/10.1126/science.aah6412
20. Murray KO, Clanton TL, Horowitz M. Epigenetic responses to heat: from adaptation to maladaptation. *Exp Physiol* 2022;**107**:1144–58. https://doi.org/10.1113/EP090143
21. Izu H, Inouye S, Fujimoto M *et al.* Heat shock transcription factor 1 is involved in quality-control mechanisms in male germ cells. *Biol Reprod* 2004;**70**:18–24. https://doi.org/10.1095/biolreprod.103.020065
22. Kim B, Park K, Rhee K. Heat stress response of male germ cells. *Cell Mol Life Sci* 2013;**70**:2623–36. https://doi.org/10.1007/s00018-012-1165-4
23. Hutvagner G, Simard MJ. Argonaute proteins: key players in RNA silencing. *Nat Rev Mol Cell Biol* 2008;**9**:22–32. https://doi.org/10.1038/nrm2321
24. Meister G. Argonaute proteins: functional insights and emerging roles. *Nat Rev Genet* 2013;**14**:447–59. https://doi.org/10.1038/nrg3462
25. Felix MA, Ashe A, Piffaretti J *et al.* Natural and experimental infection of *Caenorhabditis nematodes* by novel viruses related to nodaviruses. *PLoS Biol* 2011;**9**:e1000586. https://doi.org/10.1371/journal.pbio.1000586
26. Lu R, Maduro M, Li F *et al.* Animal virus replication and RNAi-mediated antiviral silencing in *Caenorhabditis elegans*. *Nature* 2005;**436**:1040–3. https://doi.org/10.1038/nature03870
27. Rechavi O, Minevich G, Hobert O. Transgenerational inheritance of an acquired small RNA-based antiviral response in *C. elegans*. *Cell* 2011;**147**:1248–56. https://doi.org/10.1016/j.cell.2011.10.042
28. Wilkins C, Dishongh R, Moore SC *et al.* RNA interference is an antiviral defence mechanism in *Caenorhabditis elegans*. *Nature* 2005;**436**:1044–7. https://doi.org/10.1038/nature03957
29. Rechavi O, Houri-Ze'evi L, Anava S *et al.* Starvation-induced transgenerational inheritance of small RNAs in *C. elegans*. *Cell* 2014;**158**:277–87. https://doi.org/10.1016/j.cell.2014.06.020
30. Zhang X, Zabinsky R, Teng Y *et al.* microRNAs play critical roles in the survival and recovery of *Caenorhabditis elegans* from starvation-induced L1 diapause. *Proc Natl Acad Sci USA* 2011;**108**:17997–8002. https://doi.org/10.1073/pnas.1105982108
31. Seroussi U, Lugowski A, Wadi L *et al.* A comprehensive survey of *C. elegans* argonaute proteins reveals organism-wide gene regulatory networks and functions. *eLife* 2023;**12**:e83853. https://doi.org/10.7554/eLife.83853
32. Cecere G, Hoersch S, O'Keeffe S *et al.* Global effects of the CSR-1 RNA interference pathway on the transcriptional landscape. *Nat Struct Mol Biol* 2014;**21**:358–65. https://doi.org/10.1038/nsmb.2801
33. Claycomb JM, Batista PJ, Pang KM *et al.* The Argonaute CSR-1 and its 22G-RNA cofactors are required for holocentric chromosome segregation. *Cell* 2009;**139**:123–34. https://doi.org/10.1016/j.cell.2009.09.014
34. Conine CC, Moresco JJ, Gu W *et al.* Argonautes promote male fertility and provide a paternal memory of germline gene expression in C. elegans. *Cell* 2013;**155**:1532–44. https://doi.org/10.1016/j.cell.2013.11.032
35. Gerson-Gurwitz A, Wang S, Sathe S *et al.* A small RNA-catalytic argonaute pathway tunes germline transcript levels to ensure embryonic divisions. *Cell* 2016;**165**:396–409. https://doi.org/10.1016/j.cell.2016.02.040
36. Quarato P, Singh M, Cornes E *et al.* Germline inherited small RNAs facilitate the clearance of untranslated maternal mRNAs in *C. elegans* embryos. *Nat Commun* 2021;**12**:1441. https://doi.org/10.1038/s41467-021-21691-6
37. Seth M, Shirayama M, Gu W *et al.* The *C. elegans* CSR-1 argonaute pathway counteracts epigenetic silencing to promote germline gene expression. *Dev Cell* 2013;**27**:656–63. https://doi.org/10.1016/j.devcel.2013.11.014
38. Charlesworth AG, Seroussi U, Lehrbach NJ *et al.* Two isoforms of the essential *C. elegans* Argonaute CSR-1 differentially regulate sperm and oocyte fertility. *Nucleic Acids Res* 2021;**49**:8836–65. https://doi.org/10.1093/nar/gkab619
39. Nguyen DAH, Phillips CM. Arginine methylation promotes siRNA-binding specificity for a spermatogenesis-specific isoform of the Argonaute protein CSR-1. *Nat Commun* 2021;**12**:4212. https://doi.org/10.1038/s41467-021-24526-6

40. Girard LR, Fiedler TJ, Harris TW *et al.* WormBook: the online review of *Caenorhabditis elegans* biology. *Nucleic Acids Res* 2007;**35**:D472–5. https://doi.org/10.1093/nar/gkl894
41. Kiontke K, Fernandez P, Woronik A *et al.* Morphologically defined substages of tail morphogenesis in *C. elegans* males. *Developmental Dynamics* 2024;**253**:1147–64. https://doi.org/10.1002/dvdy.721
42. Soete G, Betist MC, Korswagen HC. Regulation of *Caenorhabditis elegans* body size and male tail development by the novel gene lon-8. *BMC Dev Biol* 2007;**7**:20. https://doi.org/10.1186/1471-213X-7-20
43. Manjarrez JR, Mailler R. Stress and timing associated with *Caenorhabditis elegans* immobilization methods. *Heliyon* 2020;**6**:e04263. https://doi.org/10.1016/j.heliyon.2020.e04263
44. Zevian SC, Yanowitz JL. Methodological considerations for heat shock of the nematode *Caenorhabditis elegans*. *Methods* 2014;**68**:450–7. https://doi.org/10.1016/j.ymeth.2014.04.015
45. Dokshin GA, Ghanta KS, Piscopo KM *et al.* Robust genome editing with short single-stranded and long, partially single-stranded DNA donors in *Caenorhabditis elegans*. *Genetics* 2018;**210**:781–7. https://doi.org/10.1534/genetics.118.301532
46. Stinchcomb DT, Shaw JE, Carr SH *et al.* Extrachromosomal DNA transformation of *Caenorhabditis elegans*. *Mol Cell Biol* 1985;**5**:3484–96.
47. Kurhanewicz NA, Dinwiddie D, Bush ZD *et al.* Elevated temperatures cause transposon-associated DNA damage in *C. elegans* spermatocytes. *Curr Biol* 2020;**30**:5007–17. https://doi.org/10.1016/j.cub.2020.09.050
48. Reboul J, Vaglio P, Rual JF *et al. C. elegans* ORFeome version 1.1: experimental verification of the genome annotation and resource for proteome-scale protein expression. *Nat Genet* 2003;**34**:35–41. https://doi.org/10.1038/ng1140
49. Zhang S, Banerjee D, Kuhn JR. Isolation and culture of larval cells from *C. elegans*. *PLoS One* 2011;**6**:e19505. https://doi.org/10.1371/journal.pone.0019505
50. Liu P, Shi J, Sheng D *et al.* Mitopherogenesis, a form of mitochondria-specific ectocytosis, regulates sperm mitochondrial quantity and fertility. *Nat Cell Biol* 2023;**25**:1625–36. https://doi.org/10.1038/s41556-023-01264-z
51. Mata-Cabana A, Sin O, Seinstra RI *et al.* Nuclear/cytoplasmic fractionation of proteins from *Caenorhabditis elegans*. *Bio-Protocol* 2018;**8**:e3053. https://doi.org/10.21769/BioProtoc.3053
52. Zheng Y. CUT&Tag Data Processing and Analysis Tutorial. *Protocol.io* 2020;**1**:e63274.
53. Zhang L, Ward JD, Cheng Z *et al.* The auxin-inducible degradation (AID) system enables versatile conditional protein depletion in *C. elegans*. *Development* 2015;**142**:4374–84.
54. Jaramillo-Lambert A, Ellefson M, Villeneuve AM *et al.* Differential timing of S phases, X chromosome replication, and meiotic prophase in the *C. elegans* germ line. *Dev Biol* 2007;**308**:206–21. https://doi.org/10.1016/j.ydbio.2007.05.019
55. Campos EI, Stafford JM, Reinberg D. Epigenetic inheritance: histone bookmarks across generations. *Trends Cell Biol* 2014;**24**:664–74. https://doi.org/10.1016/j.tcb.2014.08.004
56. Lacal I, Ventura R. Epigenetic inheritance: concepts, mechanisms and perspectives. *Front Mol Neurosci* 2018;**11**:292. https://doi.org/10.3389/fnmol.2018.00292
57. Xiao Y, Bedet C, Robert VJ *et al.* Caenorhabditis elegans chromatin-associated proteins SET-2 and ASH-2 are differentially required for histone H3 Lys 4 methylation in embryos and adult germ cells. *Proc Natl Acad Sci USA* 2011;**108**:8305–10. https://doi.org/10.1073/pnas.1019290108
58. Rechtsteiner A, Ercan S, Takasaki T *et al.* The histone H3K36 methyltransferase MES-4 acts epigenetically to transmit the memory of germline gene expression to progeny. *PLoS Genet* 2010;**6**:e1001091. https://doi.org/10.1371/journal.pgen.1001091
59. Gaydos LJ, Rechtsteiner A, Egelhofer TA *et al.* Antagonism between MES-4 and Polycomb repressive complex 2 promotes appropriate gene expression in C. elegans germ cells. *Cell Rep* 2012;**2**:1169–77. https://doi.org/10.1016/j.celrep.2012.09.019
60. Guo Y, Yang B, Li Y *et al.* Enrichment of H3K9me2 on unsynapsed chromatin in caenorhabditis elegans does not target *de novo* sites. *G3* 2015;**5**:1865–78. https://doi.org/10.1534/g3.115.019828
61. Lee TW, David HS, Engstrom AK *et al.* Repressive H3K9me2 protects lifespan against the transgenerational burden of COMPASS activity in *C. elegans*. *eLife* 2019;**8**:e48498. https://doi.org/10.7554/eLife.48498
62. Lev I, Gingold H, Rechavi O. H3K9me3 is required for inheritance of small RNAs that target a unique subset of newly evolved genes. *eLife* 2019;**8**.40448. https://doi.org/10.7554/eLife.40448
63. Woodhouse RM, Buchmann G, Hoe M *et al.* Chromatin modifiers SET-25 and SET-32 are required for establishment but not long-term maintenance of transgenerational epigenetic inheritance. *Cell Rep* 2018;**25**:2259–72. https://doi.org/10.1016/j.celrep.2018.10.085
64. Dillon SC, Zhang X, Trievel RC *et al.* The SET-domain protein superfamily: protein lysine methyltransferases. *Genome Biol* 2005;**6**:227. https://doi.org/10.1186/gb-2005-6-8-227
65. Firestein R, Cui X, Huie P *et al.* Set domain-dependent regulation of transcriptional silencing and growth control by SUV39H1, a mammalian ortholog of Drosophila Su (var)3-9. *Mol Cell Biol* 2000;**20**:4900–9. https://doi.org/10.1128/MCB.20.13.4900-4909.2000
66. Holdermann I, Meyer NH, Round A *et al.* Chromodomains read the arginine code of post-translational targeting. *Nat Struct Mol Biol* 2012;**19**:260–3. https://doi.org/10.1038/nsmb.2196
67. Nielsen PR, Nietlispach D, Mott HR *et al.* Structure of the HP1 chromodomain bound to histone H3 methylated at lysine 9. *Nature* 2002;**416**:103–7. https://doi.org/10.1038/nature722
68. Padeken J, Methot SP, Gasser SM. Establishment of H3K9-methylated heterochromatin and its functions in tissue differentiation and maintenance. *Nat Rev Mol Cell Biol* 2022;**23**:623–40. https://doi.org/10.1038/s41580-022-00483-w
69. Wan QL, Meng X, Dai W *et al.* N (6)-methyldeoxyadenine and histone methylation mediate transgenerational survival advantages induced by hormetic heat stress. *Sci Adv* 2021;**7**:eabc3026. https://doi.org/10.1126/sciadv.abc3026
70. Han T, Manoharan AP, Harkins TT *et al.* 26G endo-siRNAs regulate spermatogenic and zygotic gene expression in *Caenorhabditis elegans*. *Proc Natl Acad Sci USA* 2009;**106**:18674–9. https://doi.org/10.1073/pnas.0906378106
71. Essig YJ, Webb SM, Sturzenbaum SR. Deletion of phytochelatin synthase modulates the metal accumulation pattern of cadmium exposed *C. elegans*. *Int J Mol Sci* 2016;**17**:257. https://doi.org/10.3390/ijms17020257
72. Vrablik TL, Huang L, Lange SE *et al.* Nicotinamidase modulation of NAD+ biosynthesis and nicotinamide levels separately affect reproductive development and cell survival in *C. elegans*. *Development* 2009;**136**:3637–46. https://doi.org/10.1242/dev.028431
73. Higuchi-Sanabria R, Paul JW 3rd, Durieux J *et al.* Spatial regulation of the actin cytoskeleton by HSF-1 during aging. *MBoC* 2018;**29**:2522–7. https://doi.org/10.1091/mbc.E18-06-0362
74. Bobylev AG, Galzitskaya OV, Fadeev RS *et al.* Smooth muscle titin forms in vitro amyloid aggregates. *Biosci Rep* 2016;**36**:e00334. https://doi.org/10.1042/BSR20160066
75. Desouza M, Gunning PW, Stehn JR. The actin cytoskeleton as a sensor and mediator of apoptosis. *BioArchitecture* 2012;**2**:75–87. https://doi.org/10.4161/bioa.20975
76. Ahrens S, Zelenay S, Sancho D *et al.* F-actin is an evolutionarily conserved damage-associated molecular pattern recognized by DNGR-1, a receptor for dead cells. *Immunity* 2012;**36**:635–45. https://doi.org/10.1016/j.immuni.2012.03.008

77. Rogalski TM, Gilbert MM, Devenport D *et al.* DIM-1, a novel immunoglobulin superfamily protein in *Caenorhabditis elegans*, is necessary for maintaining bodywall muscle integrity. *Genetics* 2003;**163**:905–15. https://doi.org/10.1093/genetics/163.3.905
78. Moore RS, Kaletsky R, Murphy CT. Piwi/PRG-1 argonaute and TGF-beta mediate transgenerational learned pathogenic avoidance. *Cell* 2019;**177**:1827–41. https://doi.org/10.1016/j.cell.2019.05.024
79. Du Toit A. Argonaute fends off invaders. *Nat Rev Micro* 2022;**20**:445. https://doi.org/10.1038/s41579-022-00753-6
80. Liu M, Huang M, Wang M *et al.* The clustered regularly interspaced short palindromic repeat system and argonaute: an emerging bacterial immunity system for defense against natural transformation? *Front Microbiol* 2020;**11**:593301. https://doi.org/10.3389/fmicb.2020.593301
81. Yang H, Bai D, Li Y *et al.* Allele-specific H3K9me3 and DNA methylation co-marked CpG-rich regions serve as potential imprinting control regions in pre-implantation embryo. *Nat Cell Biol* 2022;**24**:783–92. https://doi.org/10.1038/s41556-022-00900-4
82. Lismer A, Kimmins S. Emerging evidence that the mammalian sperm epigenome serves as a template for embryo development. *Nat Commun* 2023;**14**:2142. https://doi.org/10.1038/s41467-023-37820-2
83. Jung YH, Sauria MEG, Lyu X *et al.* Chromatin states in mouse sperm correlate with embryonic and adult regulatory landscapes. *Cell Rep* 2017;**18**:1366–82. https://doi.org/10.1016/j.celrep.2017.01.034
84. Hammoud SS, Nix DA, Zhang H *et al.* Distinctive chromatin in human sperm packages genes for embryo development. *Nature* 2009;**460**:473–8. https://doi.org/10.1038/nature08162
85. Chen Z, Djekidel MN, Zhang Y. Distinct dynamics and functions of H2AK119ub1 and H3K27me3 in mouse preimplantation embryos. *Nat Genet* 2021;**53**:551–63. https://doi.org/10.1038/s41588-021-00821-2
86. Becker JS, Nicetto D, Zaret KS. H3K9me3-dependent heterochromatin: barrier to cell fate changes. *Trends Genet* 2016;**32**:29–41. https://doi.org/10.1016/j.tig.2015.11.001
87. Nicetto D, Zaret KS. Role of H3K9me3 heterochromatin in cell identity establishment and maintenance. *Curr Opin Genet Dev* 2019;**55**:1–10. https://doi.org/10.1016/j.gde.2019.04.013
88. Wang C, Liu X, Gao Y *et al.* Reprogramming of H3K9me3-dependent heterochromatin during mammalian embryo development. *Nat Cell Biol* 2018;**20**:620–31. https://doi.org/10.1038/s41556-018-0093-4
89. Ashe A, Tauffenberger A, Parker JA. Heritable transmission of stress resistance by high dietary glucose in *Caenorhabditis elegans*. *PLoS Genet* 2014;**10**.e1004346. https://doi.org/10.1371/journal.pgen.1004346
90. Carone BR, Fauquier L, Habib N *et al.* Paternally induced transgenerational environmental reprogramming of metabolic gene expression in mammals. *Cell* 2010;**143**:1084–96. https://doi.org/10.1016/j.cell.2010.12.008
91. Ng SF, Lin RC, Laybutt DR *et al.* Chronic high-fat diet in fathers programs beta-cell dysfunction in female rat offspring. *Nature* 2010;**467**:963–6. https://doi.org/10.1038/nature09491
92. Seong KH, Li D, Shimizu H *et al.* Inheritance of stress-induced, ATF-2-dependent epigenetic change. *Cell* 2011;**145**:1049–61. https://doi.org/10.1016/j.cell.2011.05.029
93. Bao J, Bedford MT. Epigenetic regulation of the histone-to-protamine transition during spermiogenesis. *Reproduction* 2016;**151**:R55–70. https://doi.org/10.1530/REP-15-0562
94. Erkek S, Hisano M, Liang CY *et al.* Molecular determinants of nucleosome retention at CpG-rich sequences in mouse spermatozoa. *Nat Struct Mol Biol* 2013;**20**:868–75. https://doi.org/10.1038/nsmb.2599
95. Gusse M, Sautiere P, Belaiche D *et al.* Purification and characterization of nuclear basic proteins of human sperm. *Biochim Biophys Gen Sub* 1986;**884**:124–34. https://doi.org/10.1016/0304-4165(86)90235-7
96. Ribas-Maynou J, Nguyen H, Wu H *et al.* Functional aspects of sperm chromatin organization. *Results Probl Cell Differ* 2022;**70**:295–311. https://doi.org/10.1007/978-3-031-06573-6_10
97. Tanphaichitr N, Sobhon P, Taluppeth N *et al.* Basic nuclear proteins in testicular cells and ejaculated spermatozoa in man. *Exp Cell Res* 1978;**117**:347–56. https://doi.org/10.1016/0014-4827(78)90148-9
98. Dubruille R, Herbette M, Revel M *et al.* Histone removal in sperm protects paternal chromosomes from premature division at fertilization. *Science* 2023;**382**:725–31. https://doi.org/10.1126/science.adh0037
99. Shirane K, Miura F, Ito T *et al.* NSD1-deposited H3K36me2 directs de novo methylation in the mouse male germline and counteracts Polycomb-associated silencing. *Nat Genet* 2020;**52**:1088–98. https://doi.org/10.1038/s41588-020-0689-z
100. Lismer A, Siklenka K, Lafleur C *et al.* Sperm histone H3 lysine 4 trimethylation is altered in a genetic mouse model of transgenerational epigenetic inheritance. *Nucleic Acids Res* 2020;**48**:11380–93. https://doi.org/10.1093/nar/gkaa712
101. Siklenka K, Erkek S, Godmann M *et al.* Disruption of histone methylation in developing sperm impairs offspring health transgenerationally. *Science* 2015;**350**:aab2006. https://doi.org/10.1126/science.aab2006

Received: June 26, 2024. **Revised:** January 14, 2025. **Editorial Decision:** February 6, 2025. **Accepted:** February 10, 2025